Splicing events in the control of genome integrity: role of SLU7 and truncated SRSF3 proteins

Maddalen Jiménez[1,†], Raquel Urtasun[1,2,†], María Elizalde[1], María Azkona[1], M. Ujue Latasa[1], Iker Uriarte[1,3], María Arechederra[1], Diego Alignani[2,4], Marina Bárcena-Varela[1], Gloria Álvarez-Sola[1,3], Leticia Colyn[1], Eva Santamaría[1,3], Bruno Sangro[2,3,5], Carlos Rodriguez-Ortigosa[1,2,3], Maite G. Fernández-Barrena[1,2,3], Matías A. Ávila[1,2,3,*,‡] and Carmen Berasain [1,2,3,*,‡]

[1]Hepatology Program, CIMA, University of Navarra, Pamplona 31008, Spain, [2]Instituto de Investigaciones Sanitarias de Navarra-IdiSNA, Pamplona 31008, Spain, [3]CIBERehd, Instituto de Salud Carlos III, Madrid 28029, Spain, [4]Cytometry Unit, CIMA, University of Navarra, Pamplona 31008, Spain and [5]Hepatology Unit, Navarra University Clinic, Pamplona 31008, Spain

ABSTRACT

Genome instability is related to disease development and carcinogenesis. DNA lesions are caused by genotoxic compounds but also by the dysregulation of fundamental processes like transcription, DNA replication and mitosis. Recent evidence indicates that impaired expression of RNA-binding proteins results in mitotic aberrations and the formation of transcription-associated RNA–DNA hybrids (R-loops), events strongly associated with DNA injury. We identify the splicing regulator SLU7 as a key mediator of genome stability. SLU7 knockdown results in R-loops formation, DNA damage, cell-cycle arrest and severe mitotic derangements with loss of sister chromatid cohesion (SCC). We define a molecular pathway through which SLU7 keeps in check the generation of truncated forms of the splicing factor SRSF3 (SRp20) (SRSF3-TR). Behaving as dominant negative, or by gain-of-function, SRSF3-TR impair the correct splicing and expression of the splicing regulator SRSF1 (ASF/SF2) and the crucial SCC protein sororin. This unique function of SLU7 was found in cancer cells of different tissue origin and also in the normal mouse liver, demonstrating a conserved and fundamental role of SLU7 in the preservation of genome integrity. Therefore, the dowregulation of SLU7 and the alterations of this pathway that we observe in the cirrhotic liver could be involved in the process of hepatocarcinogenesis.

INTRODUCTION

The preservation of genome integrity is essential for cellular homeostasis and ultimately for the individual's survival. DNA lesions, and failure to repair them, can lead to a variety of alterations ranging from point mutations to gross chromosomal rearrangements such as deletions, translocations, inversions, duplications and even to chromosomal numerical changes (aneuploidy) [1]. An increased rate of these events is referred to as genome instability, and it has been related to the pathogenesis of ageing and neoplastic diseases, constituting one of the hallmarks of cancer [2,3]. DNA lesions may originate from the action of genotoxic compounds, including xenobiotics, endogenous metabolites and particularly by agents generating reactive oxygen species [4]. However, DNA breaks may also occur in association with DNA replication stress caused by a variety of conditions such as the topological characteristics of certain DNA regions, or dysregulated cell proliferation [5]. More recently it has also been shown that gene transcription and alterations in the expression of RNA-binding proteins are important sources of replication stress and genome instability [6–10].

We have recently demonstrated that the splicing regulator SLU7 is essential to maintain the expression and splicing of the transcriptome characteristic of the differentiated, quiescent and metabolically functional liver [11]. Importantly, we have also found that SLU7 expression is significantly downregulated in damaged liver and in hepatocellular car-

cinoma (HCC) ([12]), suggesting that SLU7 inhibition may be causally related to the hepatoinsufficiency observed in patients with chronic liver injury and in the progression of hepatocarcinogenesis ([13]). Interestingly, we also observed that although reduced, the expression of SLU7 is still retained in human HCC cells and is essential for their survival ([14]). Mechanistically we found that SLU7 is required to maintain the expression of microRNAs generated from the oncogenic cluster miR-17-92 in order to inhibit apoptosis. Importantly, this function is not restricted to liver cancer cells, being SLU7 essential for the survival of transformed cells of different origin ([14]).

Intriguingly the dependency on SLU7 for survival found in transformed cells was not observed in normal cells. One of the major differences between normal and transformed cells is their proliferative activity, and the role of spliceosome components in cell cycle progression has been clearly established ([15–17]). In the present work, we demonstrate that SLU7 is essential for cells to progress through mitosis and to maintain genome stability. We found that SLU7 knockdown results in R-loops accumulation, DNA damage induction and mitotic errors such as loss of sister chromatid cohesion (SCC). Mechanistically we unravel a molecular pathway implicating new truncated forms of the splicing factor SRSF3 (SRp20) (SRSF3-TR), the microRNA miR-17 and the regulation of sororin splicing, a central event for normal chromosome segregation ([18]). Importantly, we found that these mechanisms also operate *in vivo*. In human liver tissue, the downregulation of SLU7 expression is paralleled by an increase in the levels of SRSF3-TR isoforms. Altogether, we have gathered *in vitro* and *in vivo* evidence showing that SLU7 is essential for the preservation of chromosomal stability and DNA integrity during cell proliferation, as well as for mitosis progression. These observations, together with our findings on reduced SLU7 expression in liver disease, may contribute to understand the mechanisms of chromosomal instability, which is an early event in hepatocarcinogenesis ([19]). However, our study also identifies this splicing regulator as a new molecular target for cancer therapy, given its herein demonstrated key function in the mitotic progression of cancer cells and the induction of replication stress and mitotic catastrophe upon its inhibition ([4,20]).

MATERIALS AND METHODS

Cell culture and transfections

Human HCC cell lines PLC/PRF/5 and HepG2, human cervical carcinoma cell line HeLa and human non-small cell lung cancer cell line H358 were obtained from the ATCC, were authenticated by STR profiling and tested for mycoplasma contamination. PLC/PRF/5, HepG2 and HeLa cell lines were grown in DMEM (Gibco-Life Technology, Madrid, Spain) supplemented with 10% fetal bovine serum, glutamine and antibiotics. H358 cell line was grown in RPMI supplemented with 10% fetal bovine serum. HepaRG well-differentiated HCC human cell line was obtained from BioPredic (Rennes, France). Human hepatocytes (HumHep) were obtained from liver resections of patients with secondary tumors and were isolated and cultured as reported ([14]).

Transfections with siRNAs and microRNAs were performed with Lipofectamine RNAiMAX reagent (Invitrogen, CA, USA) following the manufacturer's instructions. Sequence of siRNAs will be provided upon request. siSLU7-1 and siSLU7-2 are two independent siRNAs. Individual siRNAs were used at 75 nM, in co-transfection at 35 nM each and in double transfections siRNAs were used at 35 nM and microRNAs at 100 nM. pMIR-report plasmids (Ambion, Applied Biosystems, USA) and RNAse H1 plasmid (RNH1), kindly provided by Dr A. Aguilera (Sevilla, Spain), were transfected with Lipofectamine 2000 (Invitrogen, CA, USA) following the manufacturer's instructions.

Plasmids and luciferase activity

The sequence corresponding to SRSF3 exon 4 (pEXON4) and the same sequence with three nucleotides mutated (QuikChange II Site-Directed Mutagenesis Kit, Stratagene, CA, USA) at the putative miR-17 seed sequence (pMut), were cloned into the pMIR-REPORT luciferase plasmid (Ambion, Applied Biosystems). Luciferase activity was determined using the Dual-Luciferase Reporter Assay System (Promega, WI, USA).

Flow cytometry

Cell-cycle profiles were determined by flow cytometry analysis using a FACS Calibur flow cytometer (BD Bioscience, CA, USA) and FxCycle™ Violet stain (Thermo Fisher Scientific, DE, USA). When indicated, cells were treated overnight with nocodazole (330 nM) (Sigma-Aldrich, MO, USA) and collected or washed several times to be collected at different time points after nocodazole release.

Chromosome spreads

Chromosome spreads were prepared as described ([21]). Briefly, cells treated with nocodazole (1 µg/ml) for 3 h were collected and incubated in 0.075M KCl solution for 20 min, fixed in methanol/acetic acid (3:1 ratio), dropped onto glass slides and stained with 5.8% Giemsa solution (Merck-Millipore, CA, USA).

Immunofluorescence

For immunofluorescence, cells were cultured on coverslips and 48 h after transfection were fixed with 4% paraformaldehyde for 15 min. Immunofluorescence was performed with anti-alpha-tubulin (Sigma-Aldrich T9026; 1:10000) and anti-SLU7 (Novus Biological NBP2-20403; 1:1000, CO, USA) antibodies as described ([14]). DNA was counterstained with DAPI (Vector Laboratories, CA, USA).

R-loops detection

For R-loops detection by immunofluorescence cells were fixed, 48–72 h after knockdown, with ice-cold methanol for 15 min and immunofluorescence was performed with S9.6 antibody (Millipore MABE1095; 1:250) alone or in combination with anti-P-Ser33-RPA32 (Bethyl A300-246A;

1:3000). DNA was counterstained with DAPI (Vector Laboratories, CA, USA). All images were captured using the Zeiss Axio Imager.M1 microscope and analyzed using ImageJ software as described (22).

For R-loops detection by slot blot, genomic DNA from PLC/PRF/5 and HeLa cell lines was extracted using the automatic Maxwell system (Promega). Five micrograms of DNA were treated with 1 mg/ml of RNase A (Roche, IN, USA) in a final volume of 20 μl for 30 min at 37°C. Half of the previous sample was treated with 1U of RNase H (New England Biolabs, USA) per microgram of DNA for 30 min at 37°C. DNA (2.5 μg) was spotted on a Nylon membrane (Scleicher & Schuell, USA) using Bio-Dot® microfiltration apparatus (BioRad, CA, USA). After UV-crosslinking $(0.12J/m^2)$ membranes were stained with methylene blue and blocked with 5% milk/TBST. RNA-DNA hybrids were detected using the mouse S9.6 antibody (1:1000, Millipore MABE1095) in 1% BSA/TBST after overnight incubation at 4°C.

R-loops formed on the 3′UTR region of the *beta-Actin* gene were detected by a modification of the non-denaturing bisulfite polymerase chain reaction (PCR) method (23,24). See scheme in Supplementary Figure S3D. Briefly, non-denatured DNA from cells transfected with siGL, siSLU7 and siSLU7+RNH1 plasmid was subjected to bisulfite conversion (EZ-DNA Methylation Gold kit, Zymo Research Company, CA, USA). PCR1 was performed using primers sense GACCAGTTGAATAAAAGTGCACACC on *ACTB* exon 6 and anti-sense GSP2 (25) outside the predicted R-loop region. Nested PCRs were performed with strand-specific primers. Nested PCR3 was performed using the described 5′pause primers used to perform DRIP (25), which therefore detect the DNA strand hybridized with the RNA and protected from conversion in the R-loop. This PCR will be positive in non-denatured bisulfite treated DNA both in the presence and in the absence of R-loops. Nested PCR2 was performed using the converted 5′pause primers, which will specifically detect the converted single DNA strand (ssDNA) present only when R-loops are formed. The specificity of PCR2 was confirmed by sequencing.

RNA isolation and PCRs

Total RNA from cell lines and tissue was extracted using the automated Maxwell system (Promega). RNA samples were treated twice with DNAse to degrade all possible traces of contaminating genomic DNA (gDNA). Reverse transcription was performed as described (26). Real time PCRs were performed using iQ SYBR Green Supermix (BioRad) in a CFX96 system (BioRad) as previously described (27). Splicing events were detected after electrophoresis of PCR products amplified with primers located on both sides of the alternated splicing event as described (12). When indicated isoform-specific primers on exon junctions were used. The bands detected after electrophoresis were sequenced to be identified and to confirm specificity. Controls included PCR reactions on RNA samples without a previous retrotranscription (-RT) reaction to exclude the amplification of contaminant gDNA (Supplementary Figure S2D and F). The

sequence of primers used in the study will be provided upon request.

Western blot analysis

For protein extraction, all cell lines were lysed in RIPA buffer or in a less stringent buffer (20 mM Tris HCl pH 8, 137 mM NaCl, 1% NP-40, 2 mM ethylenediaminetetraacetic acid (EDTA)) for the SRSF3 ISO2 (SRSF3-TR) detection. The homogenates were subjected to western blot analyses as reported (26). Antibodies used were anti-SLU7 (Novus, 1:1000), anti-PARP1 (Santa Cruz SC-7150; 1:1000, CA, USA), anti-Actin (Sigma A2066; 1:6000, MO, USA), anti-Sororin (kindly provided by Dr JM Peters, Austria), anti-SRSF3 (Thermo Fisher 33-4200; 1:500 and MBL RN080PW; 1:500, MA, USA), anti-WAPL (Cell signaling 77428S; 1:1000, MA, USA), anti-H3S10P (Cell signaling #9701; 1:1000), anti-γ-H2AX (Cell signaling #2577S; 1:1000), anti-SRSF1 (Thermo Fisher 32-4600; 1:1000), anti-MAD2 (Bethyl laboratories a300-301A-M; 1:1000, TX, USA), anti-P21 (Santa Cruz SC-397; 1:1000), anti-RNaseH1 (Thermo Fisher PA5-30974; 1:1000) and anti-V5 (Invitrogene R960-25; 1:1000).

RNA-pull down

To obtain nuclei extract, PLC/PRF/5 cells were collected in nuclear isolation buffer (1.28 M sucrose, 40 mM Tris–HCl pH 7.5, 20 mM MgCl2, 4% Triton X-100) and centrifuged at $0.6 \times g$ for 15 min at 4°C. The nuclear pellet obtained was resuspended in buffer A (150 mM KCl, 25 mM Tris pH 7.4, 5 mM EDTA, 0.5 mM DTT, 0.5% NP40, 1× Protease inhibitor cocktail, 100 U/ml RNase inhibitor) and mechanically lysed using a dounce homogenizer for final protein extraction. For liver tissue, control, cirrhosis and HCC samples were powdered in dry ice. The powder was homogenized in cold phosphate buffered saline and the nuclei extract was obtained as explained.

For RNA-pull down assay, 0.8 nmol of 5′-biotin-labeled RNA oligos (O1, O2 and mutated O1) compassing SRSF3 binding motifs 1 and 2 from sororin intron 1, were immobilized onto 50 μl of Neutroavidin beads (Thermo Scientific) in 1 × TBS (50 mM Tris–HCl [pH 7.4], 150 mM NaCl) at 4°C for 2 h, followed by overnight incubation with 2 mg of PLC/PRF/5 or liver tissue protein nuclear extract at 4°C. Beads were then washed with 1 × TBS and proteins were eluted with 40 μl of 2 × Laemmli buffer for western blot analysis.

Animal experiments

C57BL/6J male mice (Harlan) were used. The 16-week-old mice were injected i.v. with rAAVs (1 × 1011 pfu) (11). Experiments were performed 21 days after AAV injection using five animals per group and were repeated at least twice. Two-thirds partial hepatectomy (PH) and sham (SH) operations were performed as described previously (28).

Immunohistochemical staining

Immunohistochemical detection of γ-H2AX and Ki67 in paraffin embedded mouse liver tissues was carried out using

a rabbit antibody against γ-H2AX (Cell signalling #2577S; 1:1000) and a rabbit monoclonal antibody against Ki67 (Thermo Scientific RM-9106; 1:200) as described (11).

Ploidy analysis

Liver sections were deparaffinized and incubated in citrate buffer at 95°C for 20 min for antigen retrieval. Sections were incubated overnight at 4°C with anti–β-Catenin (BD Biosciences 610154, 1:400). Anti-mouse-Alexa Fluor 488 (Thermo Fisher #R37120, 1:500) was used as the secondary antibody. Hoechst 33342 (0.2 μg/ml) (Sigma-Aldrich) was included in the final wash to counterstain nuclei. Images were taken using a LEICA DMI 6000 microscope at × 20 magnification, PL APO objectives, a MicroMAX-1300Y/HS Princeton Instruments camera and Metamorph 7 software (Molecular Devices). At least 250 randomly selected fields of liver sections were imaged, corresponding to the analysis of more than 100 000 cells for nuclear ploidy analysis by a specific macro developed with ImageJ software (pixels ranging from 200 to 2500 px2) as previously described (29,30).

Human samples

Samples from patients included in the study were provided by the Biobank of the University of Navarra and were processed following standard operating procedures approved by the Ethical and Scientific Committees.

Statistical analysis

Statistical analysis was performed using the GraphPad Prism software. Data are represented as mean ± SEM or as median when indicated. When appropriate, a Mann–Whitney U-test or independent Student's t-test was used to test for statistical differences between groups. The Chi-square test was used to compared frequencies. All experiments were performed at least three times in duplicate. A P-value < 0.05 was considered significant.

RESULTS

SLU7 is required for the mitotic progression of transformed cells

We have demonstrated that SLU7 depletion induces the death of transformed cell lines of different origin without affecting the survival of normal liver cells (14). Given that spliceosome components are required for cell division (15,31) we decided to analyze the effect of SLU7 knockdown in cell-cycle progression. SLU7 knockdown induced a significant arrest in G2/M phase in the hepatoma cell lines PLC/PRF/5 and HepG2 and in HeLa and H358 cell lines from cervical carcinoma and lung cancer respectively (Figure 1A). This arrest was confirmed with two independent SLU7 siRNAs in PLC/PRF/5 and HeLa cells (Supplementary Figure S1A). Nevertheless, cell-cycle distribution was not altered in normal human hepatocytes (HumHep) and the well differentiated human hepatoma cell line HepaRG after SLU7 knockdown (Figure 1A). In agreement with this mitotic arrest we found that SLU7 knockdown markedly

impaired the ability of PLC/PRF/5 cells to resume mitotic progression after release from overnight treatment with the mitotic inhibitor nocodazole (Supplementary Figure S1B). Ten hours after nocodazole release 58% of siSLU7 cells still remained arrested at G2/M comparing to 18% of control cells (siGL). These results indicate that SLU7 is required for progression through mitosis. The mitotic arrest upon SLU7 knockdown was confirmed by an increase in the mitotic index (Figure 1B), the increased expression of the mitotic marker Ser-10 phosphorylated histone H3 (H3S10P) (Figure 1C) and the induction of mitotic arrest deficient 2 (MAD2) protein, a key component of the mitotic checkpoint (Figure 1C), in asynchronous PLC/PRF/5 and HeLa cells 48 h after transfection with siSLU7. Altogether these results demonstrate that SLU7 knockdown compromises cell-cycle progression and more particularly mitosis progression in transformed cells.

SLU7 is required for proper spindle assembly and sister chromatid cohesion: regulation of sororin splicing

In the absence of SLU7 we noticed several mitotic abnormalities (Supplementary Figure S1C). PLC/PRF/5 cells transfected with control siRNA (siGL) displayed normal metaphases 2 h after release of overnight nocodazole treatment, with chromosomes properly aligned at the metaphase plate, correct bipolar spindles and SLU7 localization excluded from DNA (Figure 2A). However, in siSLU7 transfected cells those cells with reduced SLU7 expression displayed defects in chromosome alignment with failure of chromosomes to congress at the metaphase plate and defects in spindle polarity with monopolar or multipolar spindles (Figure 2B). The maintenance of euploidy depends on the fidelity of chromosomes segregation, being aneuploidy a hallmark of most classes of solid tumors. The bipolar attachment of microtubules and the tension required to initiate anaphase depends largely on a correct SCC (32). During the last years it has been demonstrated that SCC is a process especially sensitive to alterations in the splicing machinery (18). To analyze SCC, we prepared chromosome spreads from nocodazole-arrested cells and we found that mitosis in control cells (siGL) displayed characteristic X shape chromosomes. However, most of the mitosis in the SLU7-depleted cells displayed parallel or split chromatids in PLC/PRF/5, HeLa and H358 cells (Figure 2C and Supplementary Figure S2A). This observation suggests that SLU7 is required for proper SCC. Different studies have associated reduced spliceosome activity with SCC defects due to splicing aberrations, being sororin pre-mRNA processing specially sensitive (18,21,33–35). Therefore, we decided to analyze if SLU7 regulates the splicing of sororin (Figure 2D). We found that SLU7 knockdown resulted in the accumulation of unspliced sororin pre-mRNA with increased retention of introns 1 and 2 (Figure 2E and F) using two different SLU7 siRNAs (Supplementary Figure S2B). The absence of contaminating genomic DNA was confirmed by PCR of RNA samples without retrotranscription (Supplementary Figure S2D). Accordingly, a reduction in sororin protein levels was observed in SLU7-depleted PLC/PRF/5 and HeLa cells (Figure 2G). Mechanistically, sororin antagonizes the cohesion release protein WAPL to ensure the
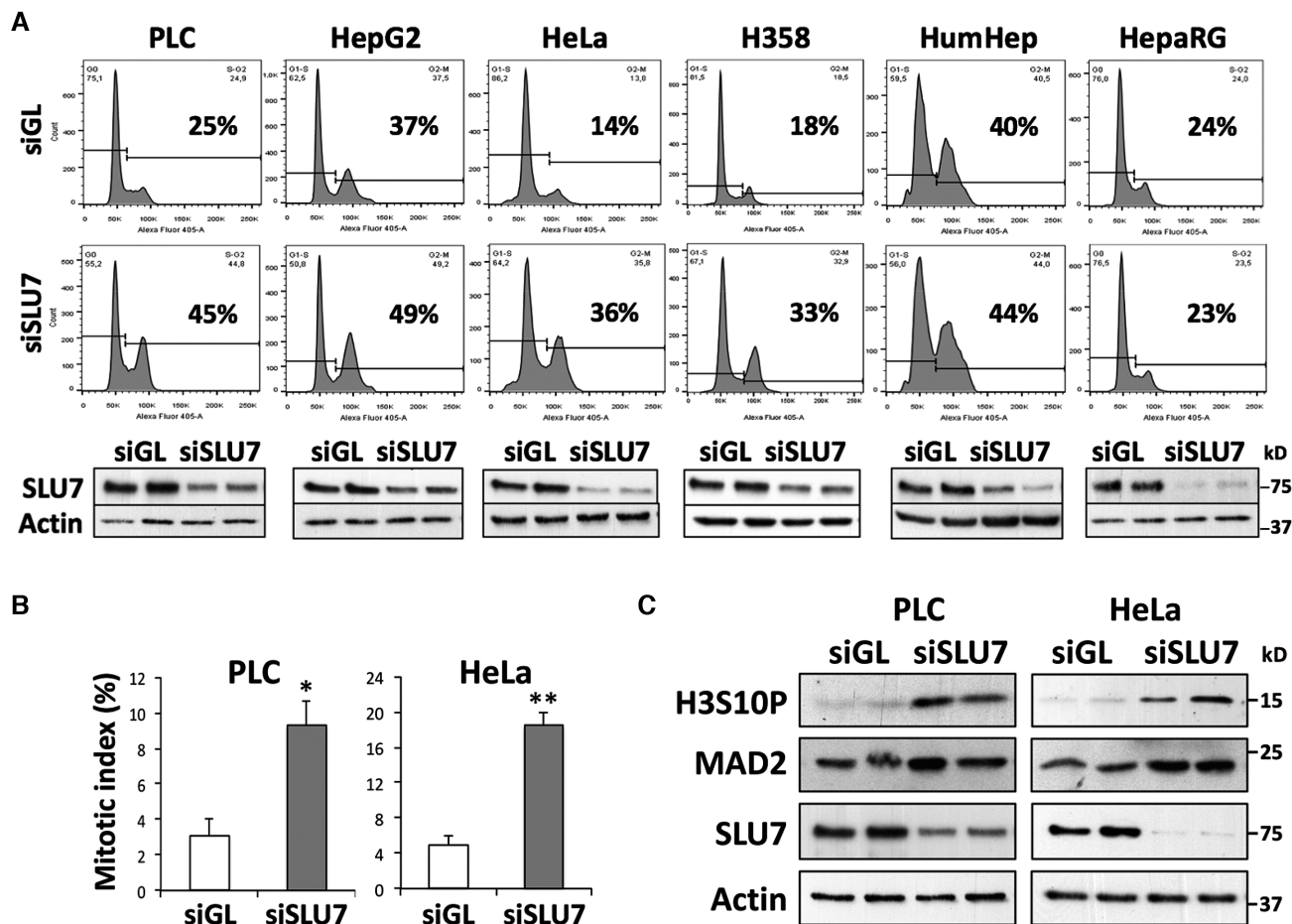
Figure 1. SLU7 is required for mitosis progression in transformed cells. (**A**) SLU7 knockdown induces cell-cycle arrest at G2/M in asynchronous transformed cells. Progression through the cell cycle was analyzed by FACS 48 h after transfection with siSLU7 or control siGL in asynchronous human hepatoma cells (PLC/PRF/5 and HepG2), the transformed cell lines HeLa (cervical carcinoma) and H358 (lung cancer), normal human hepatocytes (HumHep) and the well-differentiated human hepatoma cell line HepaRG. The percentage of cells in G2/M phase is indicated. Western blot analysis confirms SLU7 knockdown. Actin was used as loading control. At least two independent experiments of FACS analysis were performed for each cell line. (**B**) The mitotic index was calculated in asynchronous PLC/PRF/5 and HeLa cells 48 h after transfection with siSLU7 and control siGL by measuring the presence of condensed chromosomes stained with 4′,6-diamidino-2-phenylindole (DAPI). More than 250 cells per condition coming from five independent experiments performed in duplicates were counted. *$P < 0.05$, **$P < 0.01$. (**C**) Western blot analysis of the mitotic marker Ser-10 phosphorylated histone H3 (H3S10P) and the mitotic arrest deficient 2 (MAD2) protein, in PLC/PRF/5 and HeLa cells 48 h after transfection with siSLU7 and control siGL.

stable association of cohesin with chromatin (36). In fact, sororin is essential for chromatid cohesion only in the presence of WAPL (36). To confirm that SCC defects elicited after SLU7 knockdown depend largely on sororin inhibition we simultaneously silenced WAPL expression. As shown in Supplementary Figure S2G–I, co-depletion of WAPL reversed SCC defects elicited in PLC/PRF/5 cells by SLU7 knockdown.

SLU7 is required to protect cells from R-loop formation and DNA damage induction

The depletion of RNA processing factors, including the splicing factor SRSF1 (ASF/SF2), has been associated with G2/M arrest and genome instability through more direct mechanisms than SCC control, such as the formation of RNA-DNA hybrids or R-loops (6,37). R-loops contribute to genome instability in at least two ways: by the exposure of ssDNA and thus increasing the risk of DNA damage

and mutagenesis, and by inducing DNA replication stress through the impairment of replication fork progression (38,39). We have already demonstrated that SLU7 knockdown induces DNA damage in transformed cells (14) (Supplementary Figure S3A) and now we show that it also induces G2/M arrest. Therefore, we decided to analyze R-loop formation in SLU7 silenced cells. As shown in Figure 3A and B and Supplementary Figure S3B–E, by immunocytochemistry, dot-blot and non-denaturing bisulfite footprinting, we found that SLU7 knockdown leads to R-loop formation in both PLC/PRF/5 and HeLa cells, and that these R-loops are resolved in the presence of RNAse H1 (RNH1). Interestingly we also observed that the increase in γ-H2AX detected upon SLU7 knockdown was significantly reduced by RNase H1 transfection (Figure 3C), suggesting that DNA damage induced by SLU7 knockdown depends largely on R-loop formation. Accordingly, phosphorylated replication protein A (RPA), an ssDNA-binding heterotrimeric complex sensor of DNA damage,
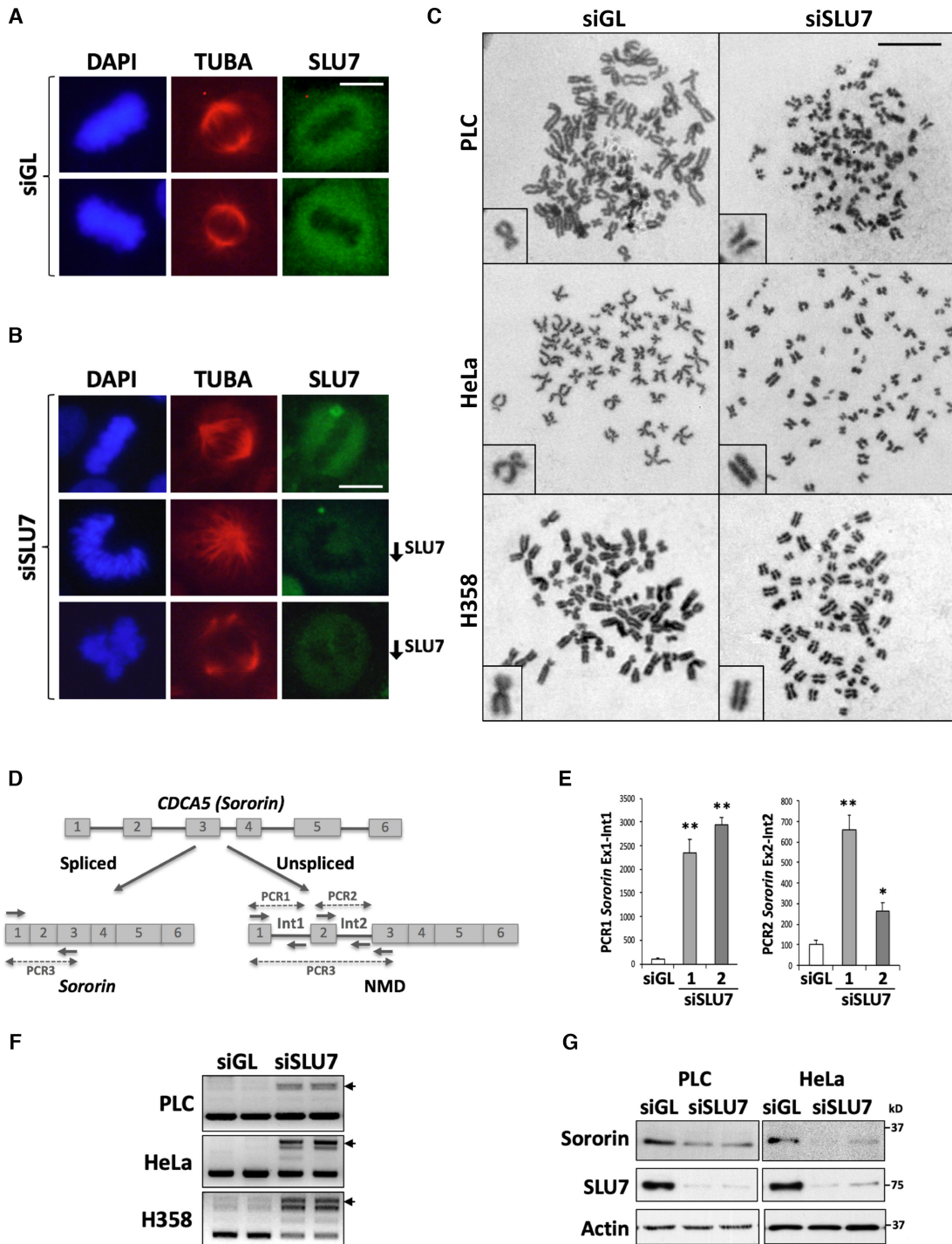
Figure 2. SLU7 is required for proper spindle assembly and SCC. (**A**) Metaphases were analyzed by immunofluorescence in PLC/PRF/5 cells 48 h after transfection with control siGL and 2 h after release of overnight treatment with nocodazole. Immunodetection of SLU7 expression and localization is shown in green, the mitotic spindle was visualized with anti-α-Tubulin (TUBA) antibody (red) and DNA was stained with DAPI (blue). Scale bar: 10 μm. (**B**) Cells transfected with siSLU7 were treated as in A. Cells with normal levels of SLU7 presented their chromosomes aligned in the metaphase plate and normal spindles as control siGL cells. Cells with reduced SLU7 levels (↓SLU7) showed abnormal (monopolar or multipolar) spindle morphology. Scale bar: 10 μm. (**C**) Representative images of metaphase chromosome spreads from PLC/PRF/5, HeLa and H358 cells 48 h after transfection with siGL or siSLU7. Scale bar: 10 μm. (**D**) Schematic representation of the genomic locus of human *CDCA5* (sororin) gene and the transcripts generated after the correct splicing or the aberrant retention of introns 1 and 2. The location of primers used for PCR1, PCR2 and PCR3 is indicated. (**E**) Real time quantification of the incorporation of intron 1 (PCR1) and intron 2 (PCR2) into *sororin* mRNA in PLC/PRF/5 cells 48 h after transfection with two different SLU7-specific siRNAs. *$P < 0.05$, **$P < 0.01$. (**F**) Analysis of *sororin* transcripts using PCR3 as described in D, in PLC/PRF/5, HeLa and H358 cells 48 h after transfection with siSLU7. Arrows indicate the aberrant intron-incorporating isoforms. (**G**) Western blot of sororin and SLU7 in PLC/PRF/5 and HeLa cells 48 h after transfection with siSLU7. Actin expression is shown as loading control. All experiments were performed at least three times with biological duplicates per condition.
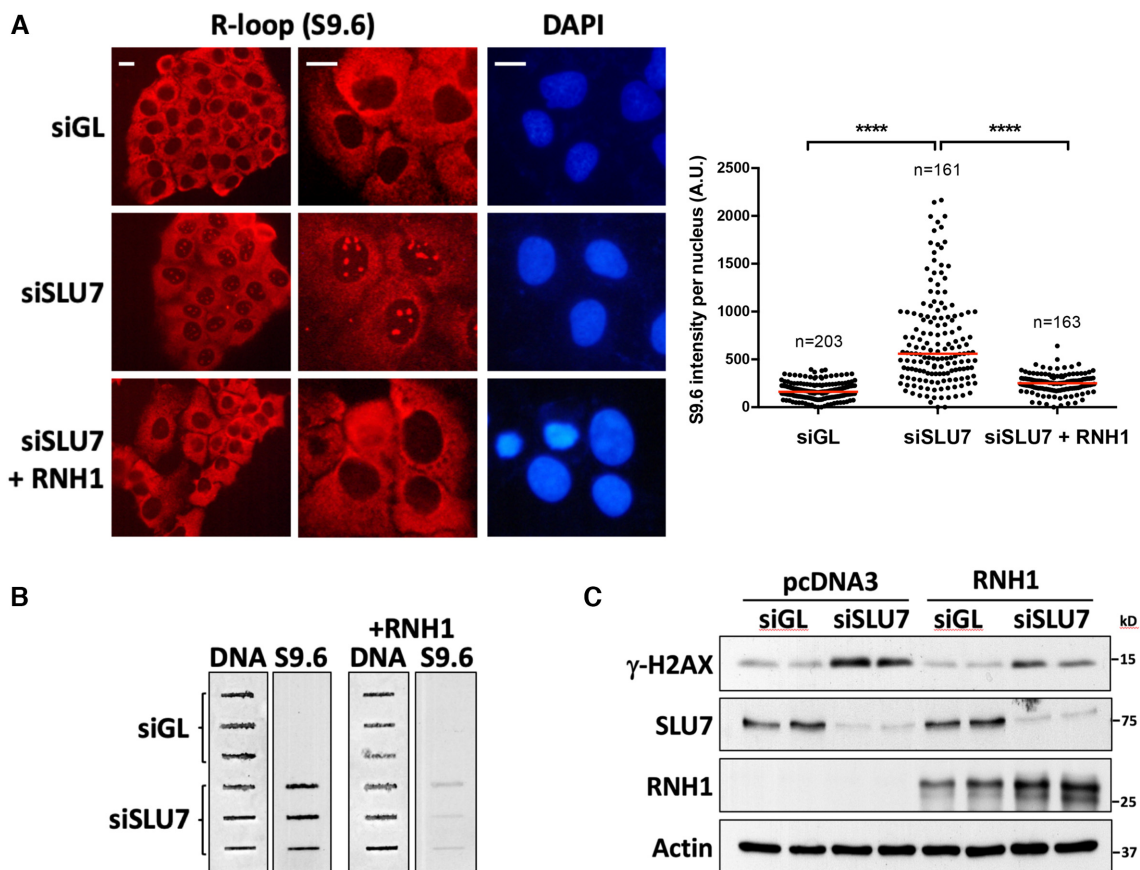
Figure 3. SLU7 protects from R-loop formation and DNA damage induction. (**A**) PLC/PRF/5 cells were probed for R-loops using the S9.6 antibody 48 h after siSLU7 transfection. Cells were transfected with a RNase H1 (RNH1) expressing plasmid to resolve R-loops as control. Nuclei were stained with DAPI. Scale bar: 10 μm. The right panel shows the quantification of RNA–DNA hybrids (R-loops) per nucleus with ImageJ software. The DAPI signal was used to create a mask of the nucleus. The nuclear S9.6 signal intensity was then determined. The number of nucleus analyzed per condition is indicated. The plot was represented using GraphPad Prism. Red bars represent the median. ****$P < 0.0001$ (Mann–Whitney U-test). (**B**) Slot-blot analysis of R-loops using S9.6 antibody in genomic DNA from PLC/PRF/5 cells 48 h after transfection with siGL or siSLU7. Right panels show the same analysis using genomic DNA after treatment with RNAse H1 as control (+RNH1). DNA was stained with methylene blue to show equal loading. (**C**) Western blot analysis of γ-H2AX and SLU7 in PLC/PRF/5 cells 48 h after transfection with siGL or siSLU7, and a control plasmid (pcDNA3) or a plasmid expressing RNase H1 (RNH1). Actin expression is shown as loading control. All experiments were performed at least three times with biological duplicates per condition.

replication stress and R-loops (40), was significantly increased upon SLU7 knockdown in PLC/PRF/5 cells, reduced upon RNase H1 transfection (Supplementary Figure S3F) and colocalized with R-loops (Supplementary Figure S3G). We next asked whether SLU7 knockdown also induced transcription-associated genomic instability in the non-tumorigenic cell line HepaRG. As shown in Supplementary Figure S3H and I we were able to detect R-loops formation, in parallel with an increase of γ-H2AX in siSLU7 transfected cells, thus confirming the relevance of SLU7 in maintaining genome integrity.

SLU7 controls *SRSF1* and *SRSF3* splicing and prevents the expression of truncated SRSF3 (SRSF3-TR) proteins

As it has been recently shown for other spliceosome factors (41) the absence of SLU7 could be directly responsible for the formation of R-loops. However, we have already demonstrated that SLU7 regulates SRSF3 splicing (11) and it is known that SRSF3 in turn regulates the expression of

SRSF1 (42,43), which as mentioned before has been implicated in the protection against R-loop formation (37). Therefore, we evaluated the effect of SLU7 knockdown on *SRSF1* and *SRSF3* splicing (Figure 4A and Supplementary Figure S2B–F). As shown in Figure 4B, confirming our previous findings (11), SLU7 knockdown induced the incorporation of exon 4 into *SRSF3* pre-mRNA to generate *SRSF3* isoform 2 (*SRSF3-ISO2*) in HCC cells, including HepaRG (Supplementary Figure S3I). Interestingly, this effect was also observed in HeLa and H358 cells (Figure 4B) using two different siRNAs and a *SRSF3-ISO2*-specific PCR (Supplementary Figure S2B). These results prompted us to evaluate if SLU7 effect on SRSF3 splicing was direct. To this end we performed an RNA-CLIP assay and we found that SLU7 binds *SRSF3* mRNA (Supplementary Figure S2C). Moreover, SLU7 knockdown significantly modified the splicing of *SRSF1* in the three cell lines tested, inducing the aberrant skipping of exon 4 in PLC/PRF/5 and H358 cells (Figure 4B and Supplementary Figure S2B, D and E) and the aberrant incorporation of intron 3 in HeLa
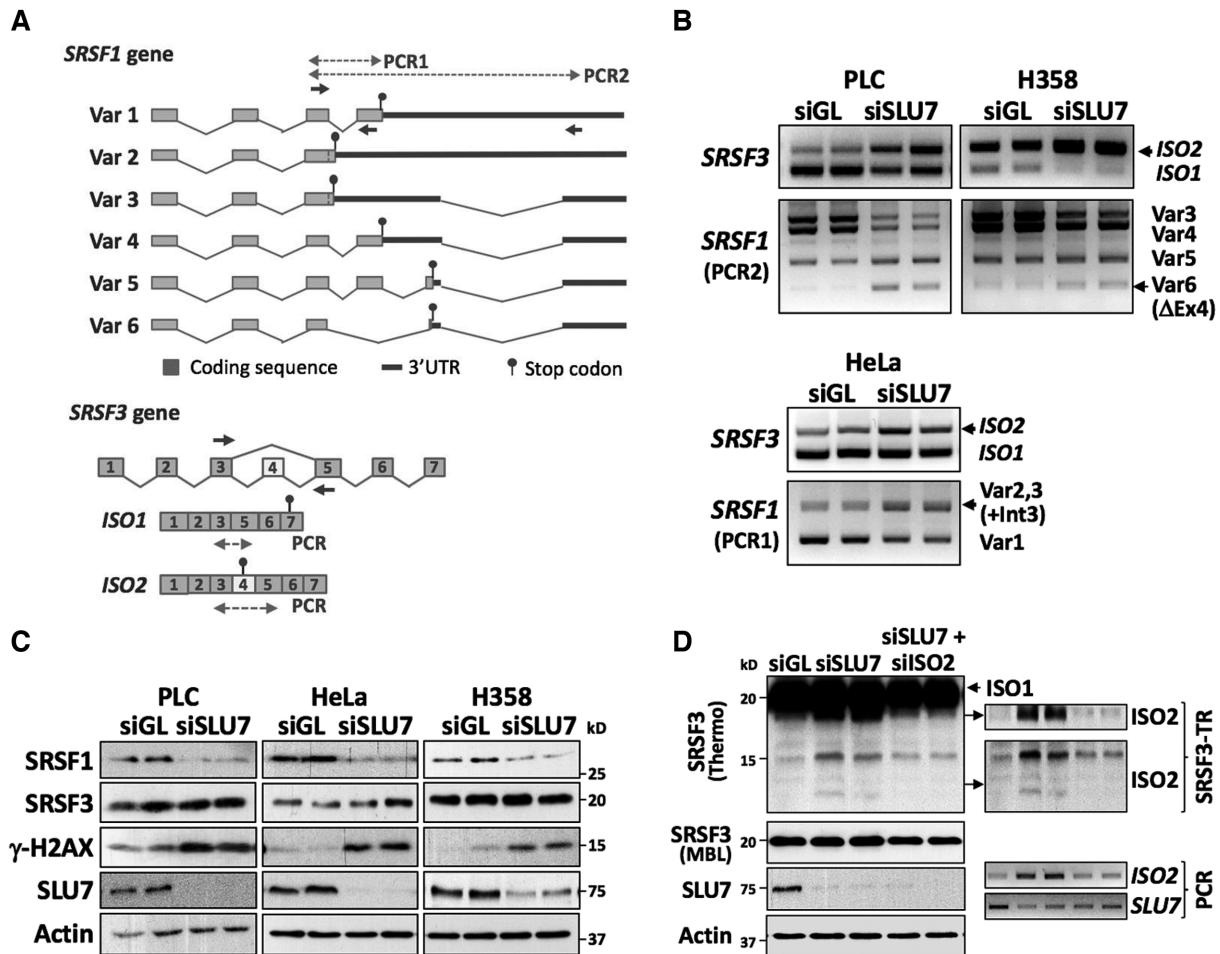
Figure 4. SLU7 controls *SRSF1* and *SRSF3* pre-mRNAs splicing and prevents the induction of SRSF3-TR forms. (**A**) Schematic representation of *SRSF1* and *SRSF3* genes and the different mRNAs generated by alternative splicing. The location of primers used for PCRs are indicated. (**B**) PCR detection of *SRSF3* and *SRSF1* isoforms 48 h after transfection with siGL or siSLU7 in the indicated cell lines. The aberrant isoforms are indicated by arrowheads. (**C**) Western blot analysis of SRSF1, SRSF3 (antibody from MBL), γ-H2AX and SLU7 in PLC/PRF/5, HeLa and H358 cells 48 h after transfection with siGL and siSLU7. Actin was used as loading control. (**D**) Western blot analysis of truncated SRSF3 forms (antibody from Thermo) in H358 cells 48 h after transfection with siGL, siSLU7 or siSLU7+siISO2. Western blot analysis of SLU7 and Actin protein levels as loading control are shown. Upper right panels show different exposures of the same membrane probed with anti-SRSF3 antibody to better identify the truncated SRSF3 forms. Lower right panels show the RT-PCR analysis of *SRSF3-ISO2* and *SLU7* mRNAs. All experiments were performed at least three times with biological duplicates per condition.

cells (Figure 4B; Supplementary Figure S2B and F). Consequently, these splicing alterations significantly reduced the expression of SRSF1 protein in the three cell lines (Figure 4C). However, SRSF3 protein levels were not affected (Figure 4C). *SRSF3-ISO2* mRNA incorporates a premature termination codon (PTC) and would be degraded by the nonsense-mediated mRNA decay (NMD) system. However, it has been shown that this isoform can be also translated into a truncated protein which lacks part of the RS domain (SRSF3-TR) (44,45). Therefore, we decided to re-evaluate SRSF3 expression with another antibody induced against a peptide epitope (aa 84–104 from Thermo Fisher) that should be contained in all the isoforms. As shown in Figure 4D, we found that upon SLU7 knockdown several truncated SRSF3 forms (SRSF3-TR) were detected. Interestingly, all SRSF3-TR forms would be expressed from *SRSF3-ISO2* mRNA, as they were inhibited when upregulation of SRSF3-ISO2 mRNA was prevented by the co-

transfection of siSLU7 with a SRSF3 exon 4 specific siRNA (siISO2) (Figure 4D and Supplementary Figure S4A). In all, our results demonstrate that SLU7 is essential to maintain the correct splicing of *SRSF1* and *SRSF3*, and to prevent the expression of truncated SRSF3 proteins.

SRSF3-TR proteins induced upon SLU7 knockdown may function as SRSF3 dominant negative and regulate SRSF1 expression and R-loop formation

In view of the above findings, we decided to evaluate the implication of *SRSF3-ISO2* and SRSF3-TR in the alteration of *SRSF1* splicing and R-loop formation induced upon SLU7 knockdown. As shown in Figure 5A, prevention of *SRSF3-ISO2* upregulation by co-transfection of siSLU7 with siISO2 in PLC/PRF/5 and HeLa cells (Supplementary Figure S4A), corrected the splicing alterations of *SRSF1* induced upon SLU7 knockdown. This effect was translated
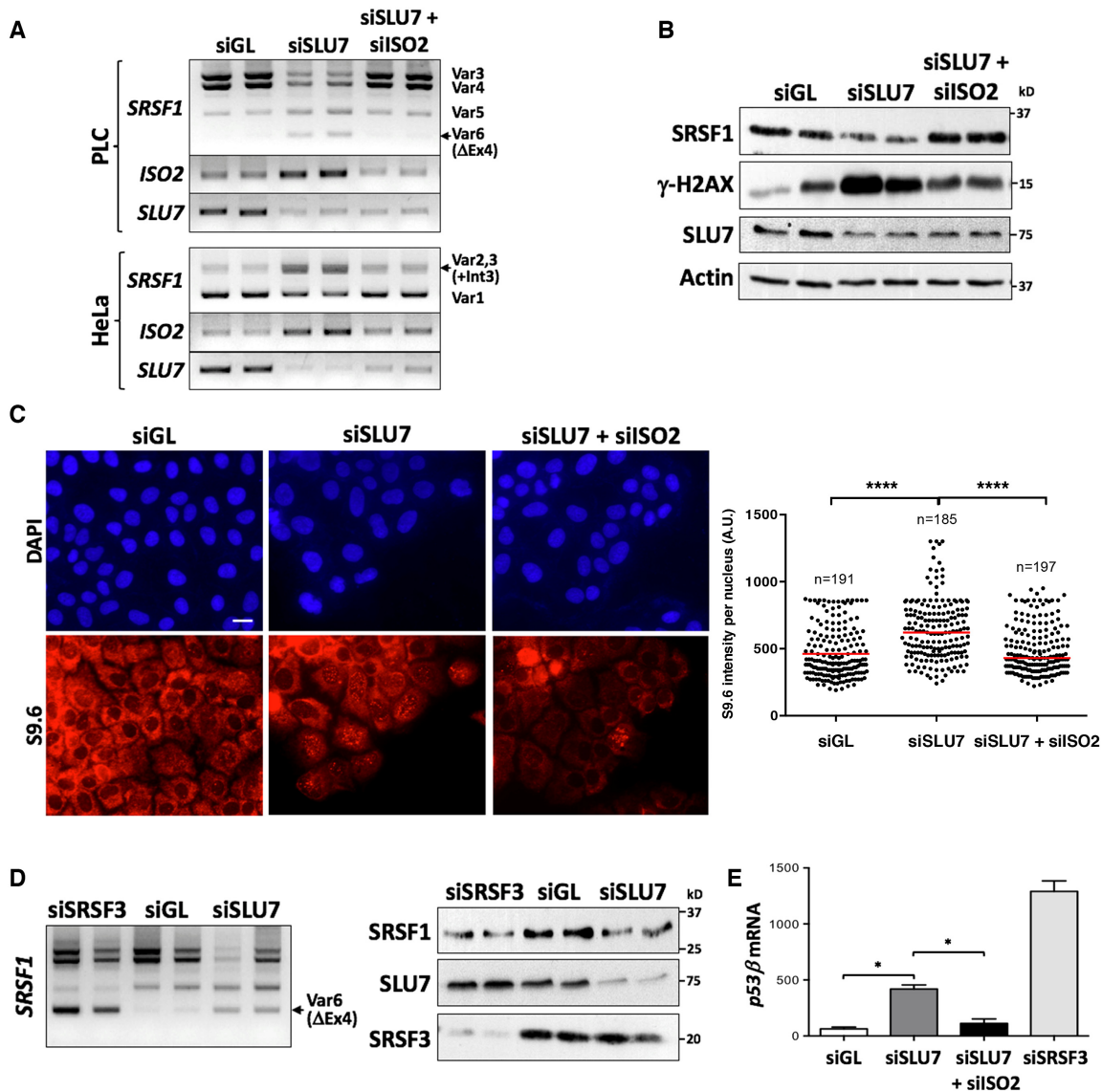
Figure 5. SRSF3-TR forms induced upon SLU7 knockdown behave as dominant-negative controlling *SRSF1* splicing and R-loops. (**A**) The generation of aberrant splice variants of SRSF1 induced upon SLU7 knockdown (siSLU7) in PLC/PRF/5 and HeLa cells is prevented by co-transfection with siISO2 targeting the truncated forms of SRSF3. The expression of *SRSF3-ISO2* and *SLU7* is shown as control. (**B**) The downregulation of SRSF1 protein and the induction of DNA damage (γ-H2AX) in PLC/PRF/5 cells after SLU7 knockdown are prevented with siISO2 (samples are the same as in panel A). Western blot analysis of SLU7 and Actin are shown as control. (**C**) The induction of R-loops after SLU7 knockdown was significantly reduced after co-transfection with siISO2 in PLC/PRF/5 cells (R-loops were detected by immunofluorescence with the S9.6 antibody). Scale bar: 10 μm. The right panel shows the quantification of RNA–DNA hybrids (R-loops) per nucleus with ImageJ software. The DAPI signal was used to create a mask of the nucleus. The nuclear S9.6 signal intensity was then determined. The number of nucleus analyzed per condition is indicated. The plot was represented using GraphPad Prism. Red bars represent the median. ****$P < 0.0001$ (Mann–Whitney U-test). (**D**) SRSF3 (siSRSF3) knockdown in PLC/PRF/5 cells results in aberrant *SRSF1* splicing and reduced protein, reproducing the effects of SLU7 (siSLU7) knockdown. Western blot analyses of SRSF1, SLU7 and SRSF3 proteins are shown. (**E**) Real time PCR of *p53* isoform beta (*p53β*) in PLC/PRF/5 cells 48 h after transfection with siSLU7, siSLU7 + siISO2 or siSRSF3. *$P < 0.05$.

into the recovery of SRSF1 protein expression and the inhibition of DNA damage induction (Figure 5B and Supplementary Figure S4B). In agreement with these results we found that preventing *SRSF3-ISO2* induction significantly reduced the accumulation of R-loops upon SLU7 knockdown (Figure 5C). Taken together these results suggest that, although SLU7 could play a direct role preventing the formation of R-loops, this effect could be also dependent on the correct expression of SRSF1 and SRSF3.

As mentioned before, it has been shown that SRSF3 depletion results in the inhibition of SRSF1 expression (42,43). However, in our system SRSF3 expression is not modified. Therefore, we hypothesized that after SLU7 knockdown, SRSF3-TR could act as a dominant negative regulator of SRSF3. To test this hypothesis, we first studied if the inhibition or knockdown of SRSF3 had the same effect on *SRSF1* splicing than siSLU7. Both SRSF3 and SLU7 knockdown reduced SRSF1 protein expression and

altered *SRSF1* splicing increasing the skipping of exon 4 in PLC/PRF/5 cells (Figure 5D) or the inclusion of intron 3 in HeLa cells (Supplementary Figure S4C). SRSF3 knockdown also induced R-loops formation in PLC/PRF/5 cells (Supplementary Figure S4D). Moreover, the splicing target of SRSF3, *p53β*, which is significantly induced upon SRSF3 knockdown (46) is also markedly induced after SLU7 knockdown, and this effect is blunted by the co-transfection of siISO2 (Figure 5E). All these results confirm that the truncated forms of SRSF3-TR elicited upon SLU7 knockdown could behave as dominant negative species toward SRSF3 activity.

SRSF3-TR proteins induced upon SLU7 knockdown regulate *sororin* splicing and SCC independently of SRSF3 inhibition

At this point it was important to analyze the role of *SRSF3-ISO2* and SRSF3-TR in the cellular phenotype induced upon SLU7 knockdown. As shown in Figure 6, we found that when the induction of *SRSF3-ISO2* was prevented (Supplementary Figure S4A) the cell-cycle arrest (Figure 6A), the defect in SCC (Figure 6B) and the apoptosis (Figure 6C) induced upon SLU7 knockdown were averted. Moreover, we also found that the aberrant splicing of *sororin* was also significantly corrected in the three cell lines tested (Figure 6D and E). However, and unexpectedly in this case the effect of SRSF3-TR proteins cannot be attributed to an inhibition of SRSF3 acting as dominant negative forms, because SRSF3 knockdown had no effect on *sororin* splicing (Figure 6F) in none of the three cell lines tested. These results suggest that the induction of *SRSF3-ISO2* could directly alter the splicing of sororin. To test this possibility, we prepared three different constructs to express the isoforms codified by *SRSF3-ISO2* (Supplementary Figure S4E and F): one ending at the end of exon 4, another construct ending at the PTC present in exon 4 and the same sequence fused to the V5 tag. We found that transfection of all three constructs into PLC/PRF/5 cells induced a significant increase in the incorporation of introns 1 and 2 in *sororin* transcripts (Figure 6G). In addition, overexpression of SRSF3-TR proteins upon *SRSF3-ISO2* transfection induced the formation of R-loops in PLC/PRF/5 (Supplementary Figure S4F). A bioinformatic analysis revealed two putative SRSF3 binding motifs (32,37) in *sororin* intron 1 (Supplementary Figure S4G). Therefore, we performed RNA-pull down assays using PLC/PRF/5 cells transfected with *SRSF3-ISO2* and two synthetic biotinylated RNA oligos containing motif 1 or motif 2. As shown in Figure 6H we found that *SRSF3-ISO2* binds the two motifs present in sororin intron 1. More importantly, we detected the binding to both oligos of the truncated SRSF3 proteins (SRSF3-TR) induced upon SLU7 knockdown in PLC/PRF/5 cells (Figure 6I). Interestingly, under these conditions the oligos were able to bind the aberrant SRSF3 isoforms induced upon SLU7 knockdown (see arrows in Figure 6I). This binding was prevented when the motif sequence in oligo 1 was mutated (Supplementary Figure S4H), thus confirming binding specificity. As these isoforms retain the RNA recognition motif (RRM) but have partially lost the RS domain implicated in the interaction with other proteins, the normal regulation of splicing by SRSF3 could be altered. In sum,

our results suggest that the truncated forms of SRSF3 can acquire new functions and therefore may participate in the induction of genome instability.

miR-17 rescues cell-cycle arrest and prevents the induction of truncated SRSF3 proteins upon SLU7 knockdown

As mentioned before, we previously demonstrated that miR-17 was able to rescue the death of transformed cells occurring upon SLU7 knockdown (14). We wondered if miR-17 would play a role in any of the events preceding cell death. We first demonstrated that miR-17 prevented the cell-cycle arrest at G2/M induced in SLU7-depleted PLC/PRF/5 (Figure 7A), HeLa and H358 (Supplementary Figure S5A) cells. As shown in Supplementary Figure S5B miR-17 also restored cell-cycle progression in SLU7-depleted PLC/PRF/5 cells after nocodazole release. In addition, normal SSC was observed after co-transfection of miR-17 with siSLU7 in PLC/PRF/5 (Figure 7B) and HeLa (Supplementary Figure S5C) cells. Importantly we found that this effect was parallel to the correction of *sororin* splicing (Figure 7C and Supplementary Figure S5D) and sororin expression (Figure 7D).

Bioinformatic analysis predicted a low score putative site for miR-17 in *SRSF3* exon 4 (Figure 7E). As mentioned before, exon 4 incorporates a PTC and it has been shown that PTC-containing mRNAs become substrates of microRNAs because the sequence downstream of the PTC acquires a 3′UTR identity (47). To verify this hypothesis, we cloned *SRSF3* exon 4 sequence (pEXON4) and this exon with the mutated seed sequence (pMut) fused to the 3′ end of the luciferase ORF in the reporter plasmid pMIR (Figure 7E). We co-transfected PLC/PRF/5 and HeLa cells with pEXON4 or pMut plasmids and the synthetic miR-17 mimic or the mock oligo as negative control. As shown in Figure 7E, miR-17 significantly reduced luciferase activity of pEXON4 plasmid, with no effect on pMut plasmid. In agreement with this we found that the induction of *SRSF3-ISO2* mRNA observed in PLC/PRF/5, HeLa and H358 cells after SLU7 knockdown was significantly prevented by miR-17 transfection (Figure 7F and Supplementary Figure S5E). Accordingly, the induction of SRSF3-TR forms upon SLU7 knockdown was inhibited by miR-17 co-transfection (Figure 7G). These results demonstrate that *SRSF3-ISO2* mRNA is a target of miR-17. We therefore decided to study if miR-17 was also able to rescue the aberrations in *SRSF1* splicing and the accumulation of R-loops induced upon SLU7 knockdown. As shown in Figure 7H and I and in agreement with the involvement of *SRSF3-ISO2* in those effects, miR-17 significantly corrected *SRSF1* splicing and R-loops formation when co-transfected with siSLU7 in PLC/PRF/5 cells.

SLU7 knockdown induces genomic instability *in vivo*

Our findings so far demonstrate that SLU7 is a gatekeeper of genomic integrity preventing the formation of R-loops and the induction of DNA damage and securing the correct segregation of chromosomes during mitosis. In view of this, it was very relevant to analyze if SLU7 played this role also *in vivo*. Although hepatocytes are quiescent cells
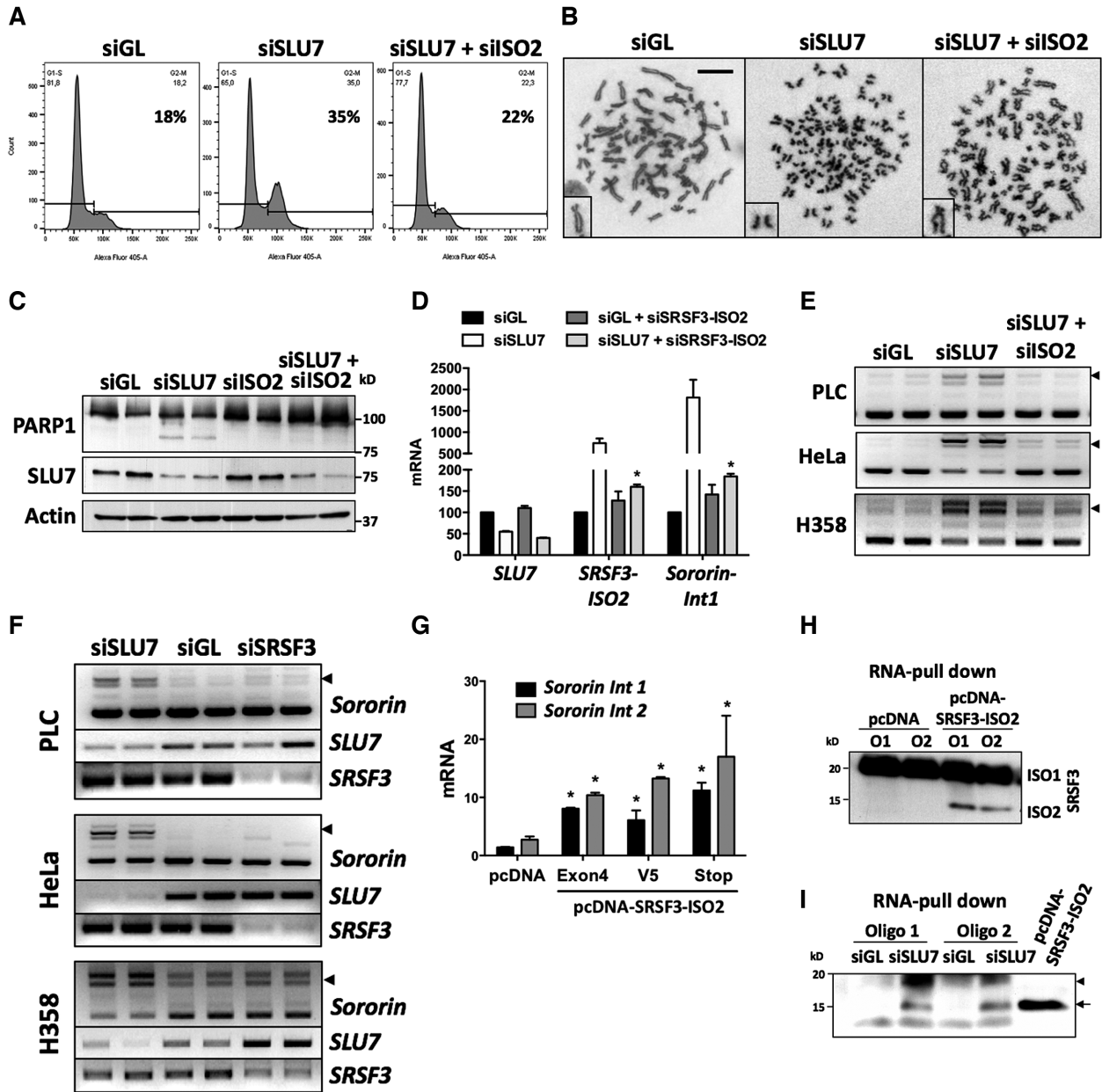
Figure 6. SLU7 knockdown-induced SRSF3-TR impair cell-cycle progression and SCC, promote apoptosis and modulate *sororin* splicing. (**A–C**) Cell-cycle arrest A, loss of SCC as detected by chromosome spreads B (scale bar: 10 μm) and apoptosis as detected by the cleavage of PARP C induced in PLC/PRF/5 cells 48 h after SLU7 knockdown were prevented by co-transfection with siISO2. (**D** and **E**) The aberrant incorporation of intron 1 in *sororin* transcripts after SLU7 knockdown in PLC/PRF/5 cells, detected by real time PCR1 D or gel electrophoresis (PCR3) E was prevented after co-transfection with siISO2. The expression of *SLU7* and *SRSF3-ISO2* is also shown in D as control. (**F**) PCR detection (PCR3 in Figure 2D) of the aberrant splicing of *sororin* (arrowheads) in PLC/PRF/5, HeLa and H358 cells 48 h after SLU7 (siSLU7) or SRSF3 (siSRSF3) knockdown. The expression of *SLU7* and *SRSF3* is shown as control. (**G**) PLC/PRF/5 cells were transfected with a control plasmid (pcDNA) or three constructs (Exon4, V5 and Stop) that overexpress *SRSF3-ISO2* mRNA (see Supplementary Figure S4E and F). The incorporation of intron 1 and intron 2 into the mRNA of *sororin* was analyzed by real time PCR1 and PCR2 (from Figure 2D). (**H**) Western blot analysis of SRSF3 after RNA-pull down using two biotinylated RNA oligos (O1 and O2) from *sororin* intron 1 containing two putative binding motifs for SRSF3. Extracts using in pull down assays were from PLC/PRF/5 cells transfected with the empty plasmid (pcDNA) or a plasmid expressing SRSF3-ISO2 (stop construct). (**I**) Western blot analysis of SRSF3 after RNA-pull down with the O1 and O2 biotinylated RNA oligos described in H using extracts from PLC/PRF/5 cells transfected with control siGL or siSLU7. The truncated isoform expressed from the pcDNA-SRSF3-ISO2 Stop construct is shown as control (arrow). The two truncated SRSF3 isoforms induced upon SLU7 knockdown (arrow and arrowhead) are able to bind both oligos. *$P < 0.05$. All experiments were performed at least three-times with biological duplicates per condition.
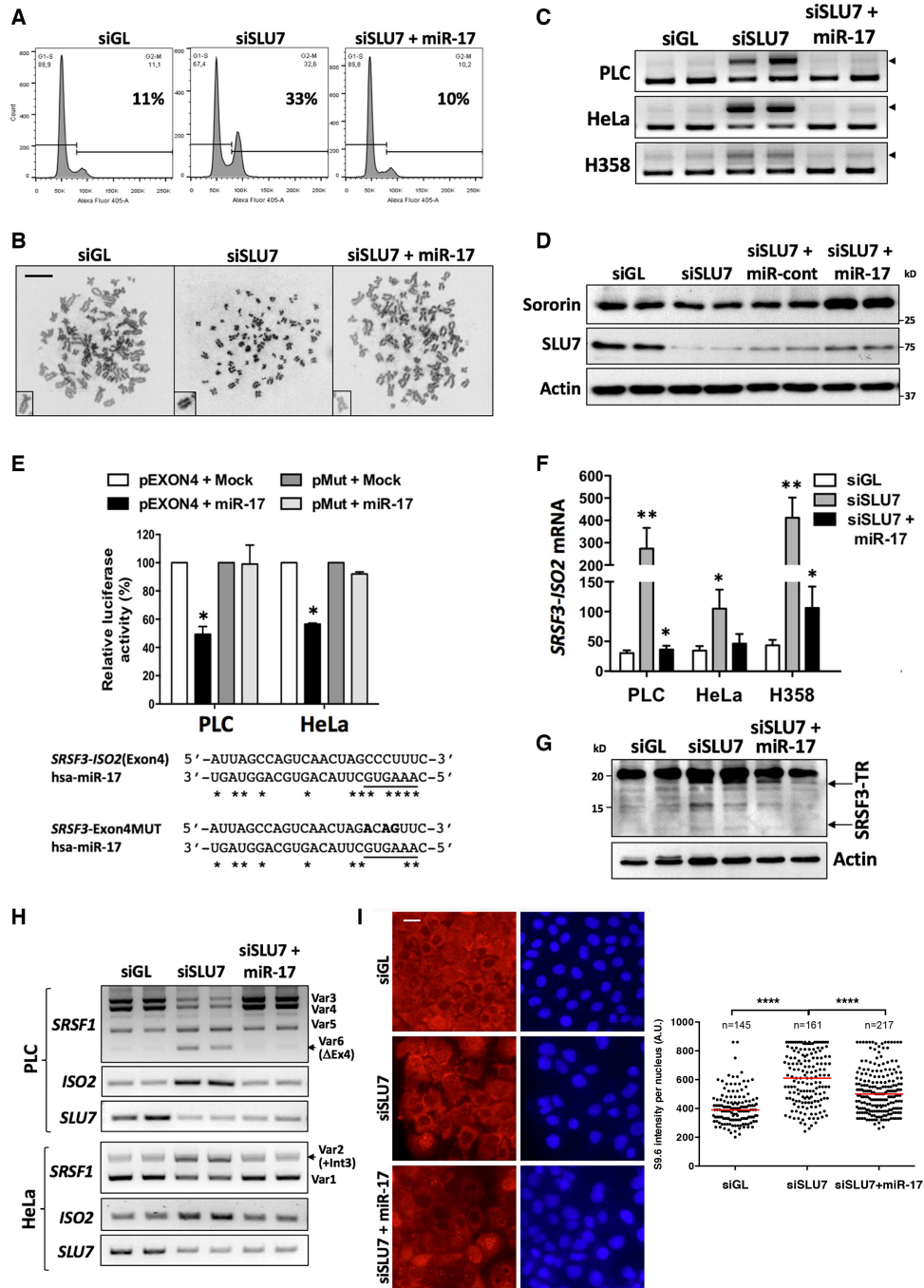
Figure 7. miR-17 rescues cell-cycle arrest and prevents the induction of SRSF3-TR proteins upon SLU7 knockdown. (**A** and **B**) Cell-cycle arrest A and loss of SCC detected by chromosome spreads B (scale bar: 10 μm) induced in PLC/PRF/5 cells 48 h after SLU7 knockdown was prevented by co-transfection with miR-17. (**C**) The aberrant splicing of *sororin* induced in PLC/PRF/5, HeLa and H358 cells 48 h after SLU7 knockdown was also prevented by co-transfection with miR-17. (**D**) Co-transfection of miR-17 with siSLU7 recovered sororin protein levels downregulated by siSLU7 in PLC/PRF/5 cells. (**E**) SRSF3 exon 4 was cloned as 3′UTR in the pMIR-REPORT luciferase plasmid (pEXON4). The same sequence with the mutations at the miR-17 recognition motif marked in bold was also cloned (pMut) as control. PLC/PRF/5 and HeLa cells were transfected with pEXON4 or pMut plasmids and miR-17 or a control miRNA (Mock). Luciferase activity was analyzed 48 h after transfection. *$P < 0.05$. (**F**) The expression of *SRSF3-ISO2* was measured by real time PCR in PLC/PRF/5, HeLa and H358 cells 48 h after transfection with siGL, siSLU7 or siSLU7 + miR-17. *$P < 0.05$, **$P < 0.01$. (**G**) Western blot analysis of SRSF3 in H358 cells 48 h after transfection with siGL, siSLU7 or siSLU7 + miR-17. The truncated forms of SRSF3 are indicated by arrows. (**H**) The generation of aberrant splice variants of *SRSF1* induced upon SLU7 knockdown (siSLU7) in PLC/PRF/5 and HeLa cells is prevented by co-transfection with miR17. The expression of *SRSF3-ISO2* and *SLU7* is shown as control. (**I**) The induction of R-loops after SLU7 knockdown was significantly reduced after co-transfection with miR-17 in PLC/PRF/5 cells (R-loops were detected by immunofluorescence with the S9.6 antibody). Scale bar: 10 μm. The right panel shows the quantification of RNA–DNA hybrids per nucleus with ImageJ software. The DAPI signal was used to create a mask of the nucleus. The nuclear S9.6 signal intensity was then determined. The number of nucleus analyzed per condition is indicated. The plot was represented using GraphPad Prism. Red bars represent the median. ****$P < 0.0001$ (Mann–Whitney U-test). All experiments were performed at least three times with biological duplicates per condition.

the liver has a unique capacity to regenerate after partial hepatectomy (PH). Our previous study demonstrated that SLU7 knockdown promotes the de-differentiation of hepatocytes and their entry into the cell cycle both in resting conditions and after PH (11). We decided to evaluate whether SLU7 is required for the correct progression through mitosis. We performed 2/3 PH in mice 21 days after knocking down SLU7 expression with an AAV encoding a SLU7-specific shRNA (AAV-shSLU7) (Supplementary Figure S6A). As shown in Figure 8A Ki67 immunostaining in sham-operated control samples (SH) confirmed the promotion of cell-cycle entrance of hepatocytes upon SLU7 knockdown. However, Ki67 immunostaining also showed that progression through mitosis after PH was significantly altered when SLU7 expression was silenced. We found that the accumulation of hepatocytes at anaphase observed in control AAV-Ren mice at the peak of mitosis, 48 h after PH (Figure 8A) was impaired in AAV-shSLU7 mice. In fact, AAV-shSLU7 mice showed an accumulation of hepatocytes arrested at prometaphase and metaphase at 48 h and even at 72 and 96 h after PH (Figure 8A). Importantly this effect was translated into a significant delay in the recovery of liver mass 96 h after PH in SLU7 knockdown mice (Figure 8B). We then analyzed sororin gene expression, finding it already induced 24 h after PH in the liver of both control AAV-Ren and AAV-shSLU7 mice (Figure 8C). However, the peak induction of *sororin* mRNA observed in AAV-Ren mice 34 h after PH was completely absent in AAV-shSLU7 mice. Interestingly, we detected an aberrant incorporation of intron 1 in *sororin* mRNA only in AAV-shSLU7 mice 24 h after PH (Figure 8C and Supplementary Figure S6B). Importantly we found that the induction of sororin protein observed in control mice (AAV-Ren) 24 h after PH was absent when SLU7 expression was knocked down (AAV-shSLU7) (Figure 8D). This effect was parallel to the onset of DNA damage (γ-H2AX levels), the activation of the spindle assembling checkpoint (SAC) evidenced by the induction of MAD2, and the induction of the major cell-cycle inhibitor P21 (Figure 8D). Together, all these results confirm *in vivo* the relevance of maintaining a correct level of expression of SLU7 to secure the normal progression through mitosis and to prevent genomic instability.

Our previous studies demonstrated that SLU7 expression is reduced in the liver of cirrhotic patients and in HCCs (12). It has also been shown that the DNA damage sensor γ-H2AX is significantly increased not only in HCC but also in the preneoplastic cirrhotic liver (48) and that DNA damage induction is associated with the development of liver cancer (19,49). We wondered if SLU7 knockdown could be associated with the development of DNA damage and genome instability in the normal resting liver. As shown in Figure 8E SLU7 knockdown in the normal liver was paralleled by the induction of DNA damage as evidenced by an increase in γ-H2AX detected by western blot (Figure 8E) and immunohistochemistry (Supplementary Figure S6C). This was also accompanied by an increase in the expression of *SRSF3-ISO2* (Figure 8E), and importantly by the alteration of hepatocyte nuclear ploidy with a trend toward a reduction in the diploid fraction and a significant increase in the octoploid fraction of hepatocytes (Figure 8F and Supplementary Figure S6D).

To explore the clinical relevance of our findings, we investigated the presence of *SRSF3-ISO2* forms in the liver of patients with cirrhosis and HCC. As shown in Figure 8G, *SRSF3-ISO2* mRNA levels were significantly elevated in human cirrhotic liver tissues and HCCs. We also performed an RNA-pull down assay with the biotinylated RNA oligo containing the putative SRSF3 binding motif 1 in sororin intron 1 described above using pooled extracts from three control livers (CO), three cirrhotic livers (CI) and three HCCs. Consistent with the observed *SRSF3-ISO2* mRNA contents, we detected increased levels of SRSF3-TR forms in the cirrhotic liver and in HCC extracts (Figure 8H). These results show for the first time that aberrant forms of SRSF3 are expressed in diseased human liver and are able to bind putative SRSF3 binding sites, in this case in the first intron of sororin.

DISCUSSION

From a mechanistic point of view, the involvement of mRNA processing factors in the maintenance of genome integrity takes place at different levels, indirectly through the regulation of the transcription and splicing of DNA damage response (DDR) and mitotic genes (9,15), or more directly through the prevention of the co-transcriptional formation of R-loops (6,9). Moreover, it has been suggested that mitotic errors and DNA damage are mechanistically separate outcomes of perturbed mRNA splicing (50). Our results confirm this hypothesis, and now we identify the splicing regulator protein SLU7 as a key factor in the preservation of genome integrity. SLU7 is an evolutionary conserved mRNA binding protein, essential during the second catalytic step in the pre-mRNA splicing process (51). Herein we define the molecular mechanisms through which SLU7 plays a non-redundant role in protecting from the accumulation of genetic lesions during fundamental events in DNA metabolism.

DNA damage, which according to Pedersen *et al.* would precede mitotic aberrations (50), would be mainly associated with the development of R-loops. Cotranscriptional R-loops, formed by the rehybridization of the nascent RNA molecule on the DNA template, are considered a major source of DNA breaks and transcription-associated genome instability (TAGIN) (10). Several studies have identified a number of RNA-binding factors that protect nascent RNA and prevent its reaction with the DNA template (6,52). One of the earliest RNA processing factors identified in this context was SRSF1 (37). Therefore, the role of SLU7 in preventing TAGIN could be mediated through its direct interaction with nascent RNA or through the preservation of the splicing and expression of other RNA processing factors like SRSF1 as we report here, albeit the coexistence of both mechanisms cannot be excluded.

We also observed profound mitotic aberrations upon SLU7 knockdown, including impaired spindle assembly, SCC and cell-cycle arrest. A central role has been established for the spliceosome machinery in the coordinated regulation of SCC during mitotic progression (18). Here also, the expression of SRSF1 was found essential for bipolar spindle formation and normal mitosis (53). Therefore, the impaired expression of SRSF1 can explain in part the
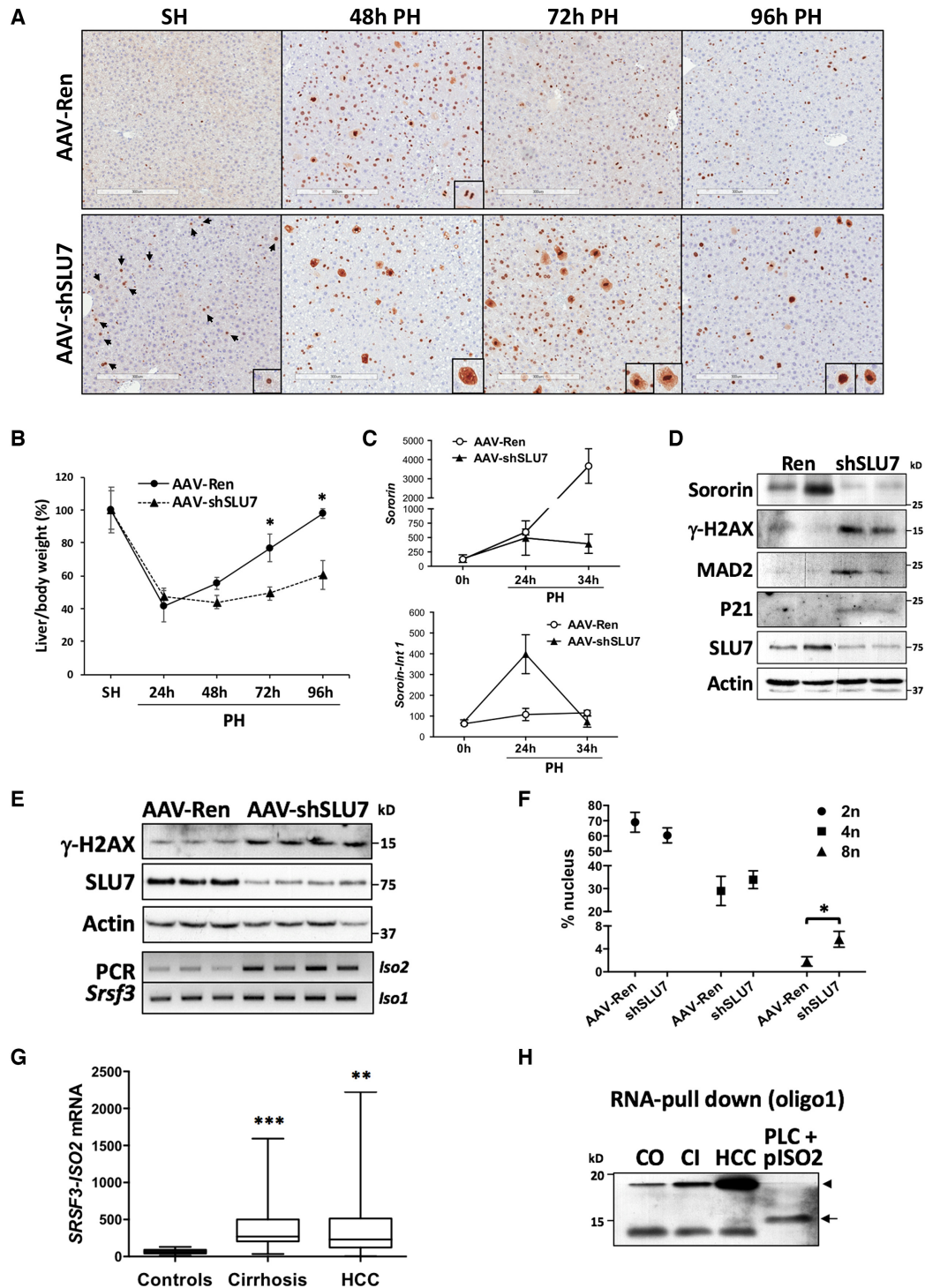
Figure 8. SLU7 knockdown induces genomic instability *in vivo*. (**A**) Ki67 immunostaining in the liver of mice 48, 72 and 96 h after 2/3 partial hepatectomy (PH) or control surgery (SH) 21 days after the injection of adenoassociated virus to inhibit SLU7 expression in the liver (AAV-shSLU7) or control virus (AAV-Ren). (*n* = 5 mice per group). (**B**) Liver to body weight ratio in AAV-shSLU7 and AAV-Ren mice 24, 48, 72 and 96 h after 2/3 partial hepatectomy (PH). (*n* = 5 mice per group). *$P < 0.05$. (**C**) Real time PCR quantification of *sororin* mRNA and intron 1-containing *sororin* transcripts in the liver of AAV-Ren and AAV-shSLU7 mice 24 and 34 h after PH. (*n* = 5 mice per group). *$P < 0.05$. (**D**) Western blot analysis of sororin, γ-H2AX, MAD2, P21, SLU7 and Actin, as loading control, in the liver of AAV-Ren and AAV-shSLU7 mice 24 h after PH. (**E**) Western blot analysis of γ-H2AX, SLU7 and Actin, as loading control, in the liver of AAV-Ren and AAV-shSLU7 mice. PCR analysis of *Srsf3 Iso1* and *Iso2* transcripts by PCR is also shown. (**F**) Quantitative analysis of hepatocyte ploidy in the liver of AAV-Ren and AAV-shSLU7. The percentage of 2n, 4n and 8n nuclei is indicated. (*n* = 4 mice per group). *$P < 0.05$. (**G**) Real time PCR quantification of *SRSF3-ISO2* expression in samples from control (*n* = 10), cirrhotic (*n* = 24) and HCC (*n* = 22) tissues. **$P < 0.01$ and ***$P < 0.001$ versus controls. (**H**) Western blot analysis of SRSF3 after RNA-pull down with the biotinylated RNA oligo O1 from sororin intron 1 containing a putative binding motif for SRSF3. Pools of three liver tissue samples from controls (CO), cirrhotic patients (CI) and HCCs were used for pull down assays. Extracts from PLC/PRF/5 cells transfected with pcDNA-SRSF3-ISO2 were included as control.

mitotic alterations found upon SLU7 knockdown. However, further to this we delineated a molecular mechanism demonstrating that SLU7 is central for the correct splicing and expression of sororin, an essential protein in cohesin ring stabilization and SCC (18,54).

While elucidating the mechanisms through which SLU7 allows normal cell-cycle progression and protects from TAGIN we also broadened the existing knowledge on the intricate regulatory crosstalk among SRSF factors (55–57). More importantly, we demonstrated that SLU7 plays a unique and hierarchically high role in this intertwined regulatory network. SR proteins can modulate splice site selection in a concentration-dependent manner (44) so their expression is tightly controlled at different levels, including their mutual control. In the case of SRSF3 it has been demonstrated that an increase in SRSF3 expression induces the incorporation of exon 4 in its own mRNA, which has been proposed as an autoregulatory mechanism to avoid SRSF3 accumulation (56). Interestingly this effect is antagonized by SRSF1, which inhibits the incorporation of *SRSF3* exon 4 (56). Here we demonstrate that the levels of SLU7 may significantly alter the expression of both SRSF1 and SRSF3. We found a marked induction of *SRSF3-ISO2* transcript upon SLU7 knockdown, which participated in the alteration of *SRSF1* splicing and reduced SRSF1 protein levels. Importantly, we were able to detect different SRSF3 truncated proteins (SRSF3-TR) coded by *SRSF3-ISO2*, which were responsible for the aberrant splicing and expression of SRSF1 and sororin. Our results demonstrate that SRSF3-TR proteins indeed play a role in the induction of DNA damage and genome instability and in the alteration of SCC. We found that these biological activities could be associated with a dominant negative effect of SRSF3-TR isoforms but also with an acquired specific function, as in the case of *sororin* splicing. Mechanistically, our findings demonstrate that SLU7 is essential to prevent an increase of SRSF3-TR proteins, acting at two different levels: by the regulation of *SRSF3* splicing and through the expression of miR-17. In this latter respect, we demonstrate that miR-17 is able to target *SRSF3-ISO2* and promote its degradation.

Our results establish that SLU7 plays a critical role in cell mitosis. In the case of hepatocytes, we previously found that an early and transient decrease in SLU7 expression is required for the hepatocytes to enter the cell cycle during liver regeneration after PH (11). Now we show that the quick recovery of SLU7 expression after PH is required to allow the correct progression through mitosis, the restoration of liver mass and the maintenance of genome stability. Importantly, our present findings demonstrate that persistent knockdown of SLU7 expression in the liver results in DNA injury and increased polyploidization, in a mechanistically significant association with enhanced *SRSF3-ISO2* levels. The preservation of normal hepatic SRSF3 function appears critical for liver homeostasis, as hepatocyte-specific deletion of this gene results in spontaneous development of liver injury and HCC (58). Together, these findings suggest that the observed downregulation of SLU7 in the cirrhotic liver (12) could participate in the induction of DNA damage, aneuploidy and genome instability which in chronic liver injury precede HCC development (19,48,59,60). The
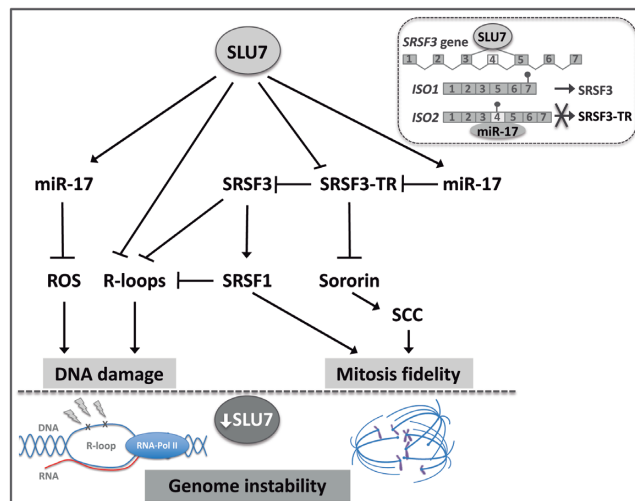

Figure 9. Schematic representation of the mechanisms regulated by SLU7 involved in the maintenance of genome integrity. See text for details.

detection of *SRSF3-ISO2* and SRSF3-TR expression in human liver cirrhosis further supports this possibility.

In the case of transformed cells, the manipulation of splicing has emerged as a potential therapeutic strategy for cancer, including drugs that inhibit early spliceosome assembly or SR protein phosphorylation (61). Importantly, pre-clinical studies show that modulating the activity of the spliceosome in general is well tolerated in vivo. Our results confirm the splicing factor SLU7 as a new target for intervention. Transformed cells demonstrate an important dependency on SLU7 expression for their survival (14), which would be related to the multiple functions of SLU7. These include the regulation of splicing and expression of SR proteins such as SRSF1 and SRSF3 and the SCC protein sororin, the prevention of R-loop formation, and the generation of microRNAs such as miR-17. The selective killing of transformed cells upon SLU7 knockdown could be associated with the induction of replication stress and mitotic catastrophe (4,20) and could be exploited for therapy.

All in all, our results demonstrate a non-redundant and hierarchical role of SLU7 in the regulation of SR proteins splicing and expression, importantly preventing the expression of SRSF3-TR isoforms. As summarized in Figure 9, the downregulation of SLU7 levels could be associated with the induction of R-loops, oxidative stress, DNA damage, mitotic aberrations and genome instability. All these events are clearly involved in the process of hepatocarcinogenesis (19). However, the dependency of transformed cells on the expression of SLU7 for their progression through mitosis could represent an 'Achilles heel' to be exploited for therapeutic intervention.

SUPPLEMENTARY DATA

Supplementary Data are available at NAR Online.

ACKNOWLEDGEMENTS

REFERENCES

1. Aguilera,A. and Gómez-González,B. (2008) Genome instability: a mechanistic view of its causes and consequences. *Nat. Rev. Genet.*, **9**, 204–217.
2. Hanahan,D. and Weinberg,R.A. (2011) Hallmarks of cancer: the next generation. *Cell*, **144**, 646–674.
3. Vogelstein,B., Papadopoulos,N., Velculescu,V.E., Zhou,S., Diaz,L.A. and Kinzler,K.W. (2013) Cancer genome landscapes. *Science*, **339**, 1546–1558.
4. Gaillard,H., García-Muse,T. and Aguilera,A. (2015) Replication stress and cancer. *Nat. Rev. Cancer*, **15**, 276–289.
5. Kotsantis,P., Petermann,E. and Boulton,S.J. (2018) Mechanisms of Oncogene-Induced replication Stress: Jigsaw falling into place. *Cancer Discov.*, **8**, 537–555.
6. Paulsen,R.D., Soni,D.V., Wollman,R., Hahn,A.T., Yee,M.-C., Guan,A., Hesley,J.A., Miller,S.C., Cromwell,E.F., Solow-Cordero,D.E. *et al.* (2009) A genome-wide siRNA screen reveals diverse cellular processes and pathways that mediate genome stability. *Mol. Cell*, **35**, 228–239.
7. Kim,N. and Jinks-Robertson,S. (2012) Transcription as a source of genome instability. *Nat. Rev. Genet.*, **13**, 204–214.
8. Brambati,A., Colosio,A., Zardoni,L., Galanti,L. and Liberi,G. (2015) Replication and transcription on a collision course: eukaryotic regulation mechanisms and implications for DNA stability. *Front. Genet.*, **6**, 166.
9. Wickramasinghe,V.O. and Venkitaraman,A.R. (2016) RNA processing and genome stability: cause and consequence. *Mol. Cell*, **61**, 496–505.
10. Gaillard,H. and Aguilera,A. (2016) Transcription as a threat to genome integrity. *Annu. Rev. Biochem.*, **85**, 291–317.
11. Elizalde,M., Urtasun,R., Azkona,M., Latasa,M.U., Goñi,S., Garcia-Irigoyen,O., Uriarte,I., Segura,V., Collantes,M., Di Scala,M. *et al.* (2014) Splicing regulator SLU7 is essential for maintaining liver homeostasis. *J. Clin. Invest.*, **124**, 2909–2920.
12. Castillo,J., Goñi,S., Latasa,M.U., Perugorría,M.J., Calvo,A., Muntané,J., Bioulac-Sage,P., Balabaud,C., Prieto,J., Avila,M.A. *et al.* (2009) Amphiregulin induces the alternative splicing of p73 into its oncogenic isoform DeltaEx2p73 in human hepatocellular tumors. *Gastroenterology*, **137**, 1805–1815.
13. Berasain,C. and Avila,M.A. (2015) Regulation of hepatocyte identity and quiescence. *Cell. Mol. Life Sci.*, **72**, 3831–3851.
14. Urtasun,R., Elizalde,M., Azkona,M., Latasa,M.U., García-Irigoyen,O., Uriarte,I., Fernandez-Barrena,M.G., Vicent,S., Alonso,M.M., Muntané,J. *et al.* (2016) Splicing regulator SLU7 preserves survival of hepatocellular carcinoma cells and other solid tumors via oncogenic miR-17-92 cluster expression. *Oncogene*, **35**, 4719–4729.
15. Hofmann,J.C., Husedzinovic,A. and Gruss,O.J. (2010) The function of spliceosome components in open mitosis. *Nucleus*, **1**, 447–459.
16. Neumann,B., Walter,T., Hériché,J.-K., Bulkescher,J., Erfle,H., Conrad,C., Rogers,P., Poser,I., Held,M., Liebel,U. *et al.* (2010) Phenotypic profiling of the human genome by time-lapse microscopy reveals cell division genes. *Nature*, **464**, 721–727.
17. Karamysheva,Z., Díaz-Martínez,L.A., Warrington,R. and Yu,H. (2015) Graded requirement for the spliceosome in cell cycle progression. *Cell Cycle*, **14**, 1873–1883.
18. Valcarcel,J. and Malumbres,M. (2014) Splicing together sister chromatids. *EMBO J.*, **33**, 2601–2603.
19. Boege,Y., Malehmir,M., Healy,M.E., Bettermann,K., Lorentzen,A., Vucur,M., Ahuja,A.K., Böhm,F., Mertens,J.C., Shimizu,Y. *et al.* (2017) A dual role of Caspase-8 in triggering and sensing Proliferation-Associated DNA damage, a key determinant of liver cancer development. *Cancer Cell*, **32**, 342–359.
20. Kotsantis,P., Jones,R.M., Higgs,M.R. and Petermann,E. (2015) Cancer therapy and replication stress: forks on the road to perdition. *Adv. Clin. Chem.*, **69**, 91–138.
21. Oka,Y., Varmark,H., Vitting-Seerup,K., Beli,P., Waage,J., Hakobyan,A., Mistrik,M., Choudhary,C., Rohde,M., Bekker-Jensen,S. *et al.* (2014) UBL5 is essential for pre-mRNA splicing and sister chromatid cohesion in human cells. *EMBO Rep.*, **15**, 956–964.
22. Hodroj,D., Recolin,B., Serhal,K., Martinez,S., Tsanov,N., Abou Merhi,R. and Maiorano,D. (2017) An ATR-dependent function for the Ddx19 RNA helicase in nuclear R-loop metabolism. *EMBO J.*, **36**, 1182–1198.
23. Yu,K., Chédin,F., Hsieh,C.-L., Wilson,T.E. and Lieber,M.R. (2003) R-loops at immunoglobulin class switch regions in the chromosomes of stimulated B cells. *Nat. Immunol.*, **4**, 442–451.
24. Sun,Q., Csorba,T., Skourti-Stathaki,K., Proudfoot,N.J. and Dean,C. (2013) R-loop stabilization represses antisense transcription at the Arabidopsis FLC locus. *Science*, **340**, 619–621.
25. Hatchi,E., Skourti-Stathaki,K., Ventz,S., Pinello,L., Yen,A., Kamieniarz-Gdula,K., Dimitrov,S., Pathania,S., McKinney,K.M., Eaton,M.L. *et al.* (2015) BRCA1 recruitment to transcriptional pause sites is required for R-loop-driven DNA damage repair. *Mol. Cell*, **57**, 636–647.
26. Perugorría,M.J., Castillo,J., Latasa,M.U., Goñi,S., Segura,V., Sangro,B., Prieto,J., Avila,M.A. and Berasain,C. (2009) Wilms' tumor 1 gene expression in hepatocellular carcinoma promotes cell dedifferentiation and resistance to chemotherapy. *Cancer Res.*, **69**, 1358–1367.
27. Castillo,J., Erroba,E., Perugorría,M.J., Santamaría,M., Lee,D.C., Prieto,J., Avila,M.A. and Berasain,C. (2006) Amphiregulin contributes to the transformed phenotype of human hepatocellular carcinoma cells. *Cancer Res.*, **66**, 6129–6138.
28. Berasain,C., García-Trevijano,E.R., Castillo,J., Erroba,E., Lee,D.C., Prieto,J. and Avila,M.A. (2005) Amphiregulin: an early trigger of liver regeneration in mice. *Gastroenterology*, **128**, 424–432.
29. Maillet,V., Boussetta,N., Leclerc,J., Fauveau,V., Foretz,M., Viollet,B., Couty,J.-P., Celton-Morizur,S., Perret,C. and Desdouets,C. (2018) LKB1 as a gatekeeper of hepatocyte proliferation and genomic integrity during liver regeneration. *Cell Rep.*, **22**, 1994–2005.
30. Gentric,G., Maillet,V., Paradis,V., Couton,D., L'Hermitte,A., Panasyuk,G., Fromenty,B., Celton-Morizur,S. and Desdouets,C. (2015) Oxidative stress promotes pathologic polyploidization in nonalcoholic fatty liver disease. *J. Clin. Invest.*, **125**, 981–992.
31. Wickramasinghe,V.O., Gonzàlez-Porta,M., Perera,D., Bartolozzi,A.R., Sibley,C.R., Hallegger,M., Ule,J., Marioni,J.C. and Venkitaraman,A.R. (2015) Regulation of constitutive and alternative mRNA splicing across the human transcriptome by PRPF8 is determined by 5′ splice site strength. *Genome Biol.*, **16**, 201.
32. Uhlmann,F. (2001) Chromosome cohesion and segregation in mitosis and meiosis. *Curr. Opin. Cell Biol.*, **13**, 754–761.
33. Sundaramoorthy,S., Vázquez-Novelle,M.D., Lekomtsev,S., Howell,M. and Petronczki,M. (2014) Functional genomics identifies a requirement of pre-mRNA splicing factors for sister chromatid cohesion. *EMBO J.*, **33**, 2623–2642.
34. van der Lelij,P., Stocsits,R.R., Ladurner,R., Petzold,G., Kreidl,E., Koch,B., Schmitz,J., Neumann,B., Ellenberg,J. and Peters,J.M. (2014) SNW1 enables sister chromatid cohesion by mediating the splicing of sororin and APC2 pre-mRNAs. *EMBO J.*, **33**, 2643–2658.

35. Watrin,E., Demidova,M., Watrin,T., Hu,Z. and Prigent,C. (2014) Sororin pre-mRNA splicing is required for proper sister chromatid cohesion in human cells. *EMBO Rep.*, **15**, 948–955.

36. Nishiyama,T., Ladurner,R., Schmitz,J., Kreidl,E., Schleiffer,A., Bhaskara,V., Bando,M., Shirahige,K., Hyman,A.A., Mechtler,K. *et al.* (2010) Sororin mediates sister chromatid cohesion by antagonizing Wapl. *Cell*, **143**, 737–749.

37. Li,X. and Manley,J.L. (2005) Inactivation of the SR protein splicing factor ASF/SF2 results in genomic instability. *Cell*, **122**, 365–378.

38. Hamperl,S. and Cimprich,K.A. (2014) The contribution of co-transcriptional RNA:DNA hybrid structures to DNA damage and genome instability. *DNA Repair (Amst.)*, **19**, 84–94.

39. Chang,E.Y.-C. and Stirling,P.C. (2017) Replication fork protection factors controlling R-Loop bypass and suppression. *Genes*, **8**, 33.

40. Nguyen,H.D., Yadav,T., Giri,S., Saez,B., Graubert,T.A. and Zou,L. (2017) Functions of replication protein A as a sensor of R loops and a regulator of RNaseH1. *Mol. Cell*, **65**, 832–847.

41. Tanikawa,M., Sanjiv,K., Helleday,T., Herr,P. and Mortusewicz,O. (2016) The spliceosome U2 snRNP factors promote genome stability through distinct mechanisms; transcription of repair factors and R-loop processing. *Oncogenesis*, **5**, e280.

42. Ajiro,M., Jia,R., Yang,Y., Zhu,J. and Zheng,Z.-M. (2015) A genome landscape of SRSF3-regulated splicing events and gene expression in human osteosarcoma U2OS cells. *Nucleic Acids Res.*, **44**, 1854–1870.

43. Muñoz,U., Puche,J.E., Hannivoort,R., Lang,U.E., Cohen-Naftaly,M. and Friedman,S.L. (2012) Hepatocyte growth factor enhances alternative splicing of the Kruppel-like factor 6 (KLF6) tumor suppressor to promote growth through SRSF1. *Mol. Cancer Res.*, **10**, 1216–1227.

44. Jumaa,H., Guénet,J.L. and Nielsen,P.J. (1997) Regulated expression and RNA processing of transcripts from the Srp20 splicing factor gene during the cell cycle. *Mol. Cell. Biol.*, **17**, 3116–3124.

45. Kano,S., Nishida,K., Kurebe,H., Nishiyama,C., Kita,K., Akaike,Y., Kajita,K., Kurokawa,K., Masuda,K., Kuwano,Y. *et al.* (2014) Oxidative stress-inducible truncated serine/arginine-rich splicing factor 3 regulates interleukin-8 production in human colon cancer cells. *Am. J. Physiol. Cell Physiol.*, **306**, C250–C262.

46. Tang,Y., Horikawa,I., Ajiro,M., Robles,A.I., Fujita,K., Mondal,A.M., Stauffer,J.K., Zheng,Z.-M. and Harris,C.C. (2013) Downregulation of splicing factor SRSF3 induces p53β, an alternatively spliced isoform of p53 that promotes cellular senescence. *Oncogene*, **32**, 2792–2798.

47. Zhao,Y., Lin,J., Xu,B., Hu,S., Zhang,X. and Wu,L. (2014) MicroRNA-mediated repression of nonsense mRNAs. *Elife*, **3**, e03032.

48. Matsuda,Y., Wakai,T., Kubota,M., Osawa,M., Takamura,M., Yamagiwa,S., Aoyagi,Y., Sanpei,A. and Fujimaki,S. (2013) DNA damage sensor γ-H2AX is increased in preneoplastic lesions of hepatocellular carcinoma. *Sci. World J.*, **2013**, 597095–597097.

49. Barash,H., Gross,E.R., Edrei,Y., Ella,E., Israel,A., Cohen,I., Corchia,N., Ben-Moshe,T., Pappo,O., Pikarsky,E. *et al.* (2010) Accelerated carcinogenesis following liver regeneration is associated with chronic inflammation-induced double-strand DNA breaks. *Proc. Natl. Acad. Sci. U.S.A.*, **107**, 2207–2212.

50. Pedersen,R.S., Karemore,G., Gudjonsson,T., Rask,M.-B., Neumann,B., Hériché,J.-K., Pepperkok,R., Ellenberg,J., Gerlich,D.W., Lukas,J. *et al.* (2016) Profiling DNA damage response following mitotic perturbations. *Nat. Commun.*, **7**, 13887.

51. Chua,K. and Reed,R. (1999) Human step II splicing factor hSlu7 functions in restructuring the spliceosome between the catalytic steps of splicing. *Genes Dev.*, **13**, 841–850.

52. Santos-Pereira,J.M., Herrero,A.B., Moreno,S. and Aguilera,A. (2014) Npl3, a new link between RNA-binding proteins and the maintenance of genome integrity. *Cell Cycle*, **13**, 1524–1529.

53. Maslon,M.M., Heras,S.R., Bellora,N., Eyras,E. and Caceres,J.F. (2014) The translational landscape of the splicing factor SRSF1 and its role in mitosis. *Elife*, **3**, e02028.

54. Ladurner,R., Kreidl,E., Ivanov,M.P., Ekker,H., Idarraga-Amado,M.H., Busslinger,G.A., Wutz,G., Cisneros,D.A. and Peters,J.M. (2016) Sororin actively maintains sister chromatid cohesion. *EMBO J.*, **35**, 635–653.

55. Änkö,M.-L., Müller-McNicoll,M., Brandl,H., Curk,T., Gorup,C., Henry,I., Ule,J. and Neugebauer,K.M. (2012) The RNA-binding landscapes of two SR proteins reveal unique functions and binding to diverse RNA classes. *Genome Biol.*, **13**, R17.

56. Jumaa,H. and Nielsen,P.J. (1997) The splicing factor SRp20 modifies splicing of its own mRNA and ASF/SF2 antagonizes this regulation. *EMBO J.*, **16**, 5077–5085.

57. Pandit,S., Zhou,Y., Shiue,L., Coutinho-Mansfield,G., Li,H., Qiu,J., Huang,J., Yeo,G.W., Ares,M. and Fu,X.-D. (2013) Genome-wide analysis reveals SR protein cooperation and competition in regulated splicing. *Mol. Cell*, **50**, 223–235.

58. Sen,S., Langiewicz,M., Jumaa,H. and Webster,N. (2015) Deletion of serine/arginine-rich splicing factor 3 in hepatocytes predisposes to hepatocellular carcinoma in mice. *Hepatology*, **61**, 171–183.

59. Toyoda,H., Bregerie,O., Vallet,A., Nalpas,B., Pivert,G., Bréchot,C. and Desdouets,C. (2005) Changes to hepatocyte ploidy and binuclearity profiles during human chronic viral hepatitis. *Gut.*, **54**, 297–302.

60. Gordon,D.J., Resio,B. and Pellman,D. (2012) Causes and consequences of aneuploidy in cancer. *Nat. Rev. Genet.*, **13**, 189–203.

61. Lee,S.C.-W. and Abdel-Wahab,O. (2016) Therapeutic targeting of splicing in cancer. *Nat. Med.*, **22**, 976–986.